EXPERIMENTAL STUDIES ON

INFILTRATION/SOIL-WATER MOVEMENT PROCESSES

AND GREEN-AMPT MODELING

A Thesis
Submitted to the Graduate Faculty
of the
North Dakota State University
of Agriculture and Applied Science

By

Leif Andrew Sande

In Partial Fulfillment of the Requirements
for the Degree of
MASTER OF SCIENCE

Major Department:
Civil Engineering

September 2011

Fargo, North Dakota

North Dakota State University
Graduate School

Title

EXPERIMENTAL STUDIES ON INFILTRATION/SOIL-WATER MOVEMENT PROCESSES AND GREEN-AMPT MODELING

By

Leif Sande

The Supervisory Committee certifies that this ***disquisition*** complies with North Dakota State University's regulations and meets the accepted standards for the degree of

MASTER OF SCIENCE

ABSTRACT

Sande, Leif Andrew. M.S., Department of Civil Engineering, College of Engineering and Architecture, North Dakota State University, September 2011. Experimental Studies on Infiltration/Soil-Water Movement Processes and Green-Ampt Modeling. Major Professor: Dr. Xuefeng Chu.

Experimental studies on infiltration/soil-water movement processes are vital to better understanding movement of soil-water in the vadose zone. The objective of this experimental research was to investigate infiltration/soil-water movement processes utilizing laboratory experiments and computer modeling. Small scale laboratory soil box infiltration experiments were conducted and utilized for the improved parameterization of the Green-Ampt (GA) saturated moisture content parameter to produce an effective moisture content parameter (θ_e) for utilization in a modified GA model. By incorporating θ_e values into GA modeling, modeling results showed greatly improved wetting front prediction across different soil conditions. A new soil packing method was proposed for replicating complex microtopographical surfaces with uniform bulk densities in laboratory soil box experiments which proved efficient and effective at accomplishing both objectives. A rainfall simulator and an instantaneous-profile laser scanner were used to simulate rainfall and quantify surface microtopography for experiments. The results clearly show the effect of microtopography on infiltration and soil-water movement characteristics. This offers valuable insight into infiltration/soil-water movement processes as affected by different soil and surface microtopographic conditions.

ACKNOWLEDGEMENTS

I would like to thank everyone who supported me, both directly and indirectly, throughout my graduate career at North Dakota State University, without which achievement of my Master's Degree would not have been feasible. Specifically, I would like to extend my thanks to my advisor, Dr. Xuefeng Chu, who provided me both the opportunity and funding to take part in this research and pursue a Master's Degree, as well as tireless guidance and assistance in conducting research and paper writing.

I would also like to extend my gratitude to my committee members: Dr. Lyle Prunty for his helpful comments and technical advice, Dr. G. Padmanabhan for his helpful comments and guidance, and especially, Dr. Thomas DeSutter for his continued and tireless support, invaluable guidance and direction, as well as his commitment and friendship.

I am also grateful to the other graduate students whose help and support was vital to the work conducted. Specifically, I would like to thank Dan Bogart, Jun Yang, Yaping Chi, and Shravan Avadhuta. I would also like to extend my thanks to Joel Bell in the Department of Soil Science for his technical assistance and support and his friendship, as well as Kyle Olson for graciously allowing us to use his farm.

I would also like to thank the faculty and staff of both the Civil Engineering and Soil Science Departments at North Dakota State University for their guidance and support.

Finally, I would also like to extend my sincerest thanks to my family for their continued and unwavering support throughout both my undergraduate and graduate career. This material is based upon the work supported by the National Science Foundation under Grant No. EAR-0907588. Without this financial support, none of this research would have been feasible.

TABLE OF CONTENTS

ABSTRACT iii

ACKNOWLEDGMENTS iv

LIST OF TABLES viii

LIST OF FIGURES ix

LIST OF SYMBOLS x

CHAPTER 1. BACKGROUND AND THESIS ORGANIZATION 1

CHAPTER 2. ESTIMATION OF EFFECTIVE WATER CONTENT USING LABORATORY EXPERIMENTAL DATA FOR IMPROVING GREEN-AMPT WETTING FRONT MODELING 4

2.1. ABSTRACT 4

2.2. INTRODUCTION AND LITERATURE REVIEW 5

2.3. METHODOLOGY 9

2.3.1. Soil Box 9

2.3.2. Soil and Soil Packing 9

2.3.3. Norton-style Rainfall Simulator 10

2.3.4. Laboratory Experiments and Data Processing 11

2.3.5. Introduction to Hydrol-Inf 13

2.3.6. Determination of GA Modeling Parameters 14

2.3.6.1. GA Capillary Suction (H_s) 15

2.3.6.2. Hydraulic Conductivity (K) 16

2.3.7. Modeling and Evaluation Procedure 18

2.4. RESULTS AND DISCUSSION 19

2.4.1. Average Effective Water Content and Saturation 19

2.4.2. GA Moisture Parameters 23

2.4.3. GA Capillary Suction Head 23

2.4.4. GA Hydraulic Conductivity 24

2.4.5. Wetting Front Movement 25

2.4.6. Ponding Time 33

2.5. CONCLUSIONS 34

CHAPTER 3. A NEW METHOD FOR REPLICATING COMPLEX MICROTOPOGRAPHIC SURFACES IN LABORATORY SOIL BOX EXPERIMENTS 36

3.1. ABSTRACT 36

3.2. INTRODUCTION AND LITERATURE REVIEW 37

3.3. METHODOLOGY 39

3.3.1. Soil Box 39

3.3.2. Surface Mold 41

3.3.3. Attaching the Surface Mold to the Soil Box 42

3.3.4. Frame and Tilting Design 43

3.3.5. Soil Packing 43

3.3.6. Instantaneous-Profile Laser Scanner 45

3.3.7. Surface Characterization and the Puddle Delineation (PD) Program 46

3.3.8. Surface Replication Procedure 47

3.4. RESULTS AND DISCUSSION 49

3.4.1. MDS and MPA 49

3.4.2. Bulk Density 50

3.5. CONCLUSIONS 51

CHAPTER 4. LABORATORY EXPERIMENTS ON THE EFFECT OF MICTROTOPOGRAPHY ON SOIL-WATER MOVEMENT: SPATIAL VARIABILITY IN WETTING FRONT MOVEMENT 54

4.1. ABSTRACT 54

4.2. INTRODUCTION AND LITERATURE REVIEW 55

4.3. METHODOLOGY 57

4.3.1. Soil Box and Soil 57

4.3.2. Surface Topography 59

4.3.3. Norton Style Rainfall Simulator 59

4.3.4. Soil Moisture 61

4.3.5. Evaluating the Effect of Microtopography on Soil-Water Movement 62

4.4. RESULTS AND DISCUSSION 63

4.4.1. The Effect of Microtopography on Soil-Water Movement Characteristics 63

4.4.1.1. Small Soil Box Experiments 63

4.4.1.2. Large Soil Box Experiments 64

4.4.2. Further Soil Water Movement Discussions 68

4.5. CONCLUSIONS 70

CHAPTER 5. OVERALL CONCLUSIONS AND FUTURE WORK 72

LITERATURE CITED 75

LIST OF TABLES

Table Page

2.1. Basic Soil Properties and Parameters 9

2.2. 15 Experiments for the Three Soil Types 12

2.3. Effective Moisture Content, Percent Saturation, and GA Modeling Effective Moisture Content for Cases 1 and 2 for all Experiments 20

2.4. Soil Hydraulic Parameters 24

2.5. Case 1 and 2 Root Mean Square Errors of Simulated from Observed Wetting Fronts, Simulated Ponding Times, and Relative Errors of Simulated from Observed Ponding Time 26

3.1. Maximum Depression Storage (MDS), Maximum Ponding Area (MPA), Standard Deviations, and Relative Errors of the Five Soil Surfaces 50

4.1. Basic Experimental Information and Soil Properties 59

4.2. Small Soil Box Final Cut Wetting Front Depths 63

4.3. Large Soil Box Wetting Front Times (t_{wet}) 64

LIST OF FIGURES

Figure Page

2.1. Actual moisture distribution during soil wetting and the Green-Ampt effective wetted zone 13

2.2. Relationships between initial moisture content θ_i and effective water content θ_e (or saturation S) for the three selected soil types 22

2.3. Comparison between the simulated and observed wetting front depths in the loamy sand soil for Cases 1 and 2 27

2.4. Comparison between the simulated and observed wetting front depths in the silty clay loam soil for Cases 1 and 2 28

2.5. Comparison between the simulated and observed wetting front depths in the silty clay soil for Cases 1 and 2 29

3.1. Soil box with attached surface molds 40

3.2. Soil box tilting schematic 44

3.3. Rough surface microtopography and bulk density core sample locations 48

4.1. Small soil box surface microtopography and soil profile cutting locations 60

4.2. Large soil box surface microtopography and moisture sensor locations at depths of 5 and 10 cm for both rough and smooth surfaces 60

4.3. Large soil box moisture sensor data for initial water content $\theta_i = 0.144$ cm^3/cm^3 for both the smooth and rough surface 65

4.4. Large soil box moisture sensor data for initial water content $\theta_i = 0.073$ cm^3/cm^3 for both the smooth and rough surface 66

LIST OF SYMBOLS

CHAPTER 2

θ = volumetric moisture content

θ_g = gravimetric moisture content

θ_i = initial moisture content

θ_s = saturated moisture content

θ_e = effective moisture content

θ_{e1} = Case 1 effective moisture content

θ_{e2} = Case 2 effective moisture content

θ_r = residual water content

λ = B & C coefficient

α' = reciprocal of P_a

ρ_b = bulk density

ρ_p = particle density

B & C = Brooks and Corey model

D = diffusivity

d_{wf} = wetting front depth at time T_w

GA = Green-Ampt model

H_s = capillary suction

K = hydraulic conductivity

K_e = effective hydraulic conductivity

K_{e1} = Case 1 effective hydraulic conductivity

K_{e2} = Case 2 effective hydraulic conductivity

K_s = saturated hydraulic conductivity

LS = loamy sand soil

RMSE = root mean square errors

n = porosity

P_c = capillary pressure

P_a = air entry pressure

r = rainfall intensity

S = percent saturation

SC = silty clay soil

SCL = silty clay loam soil

S_f = effective saturation

$t_{p,obs}$ = observed surface ponding time

t_p = time to surface ponding

t_w = time to wetting

CHAPTER 3

MDS = maximum depression storage

MPA = maximum ponding area

CHAPTER 4

θ = moisture content

θ_i = initial moisture content

ρ_b = bulk density

LS = loamy sand soil

r = rainfall intensity

t_{wet} = time wetting front to reach moisture sensor

CHAPTER 1. BACKGROUND AND THESIS ORGANIZATION

This experimental study addresses several topics in infiltration and soil-water movement processes. The study includes a variety of different scales, surface microtopography, soil textures, and moisture conditions. A modeling element is also included and the simulations are evaluated for predicting wetting front movement. The overall objective of this study is to experimentally investigate infiltration and soil-water movement processes for improving modeling of these processes for prediction purposes. Specific objectives for each chapter of his thesis are to: 1) utilize laboratory infiltration experiments for the improved parameterization of the Green-Ampt (GA) effective moisture content parameter (θ_e) for utilization in a modified GA model; 2) develop a new method for packing laboratory soil box surfaces with identical surface microtopographies and uniform bulk densities; and 3) experimentally investigate the effect of surface microtopography on soil-water movement processes utilizing differently scaled laboratory soil box experiments.

The second chapter of this thesis improves parameterization of a Green Ampt (GA) model and evaluates performance of the model at predicting wetting front movement. Laboratory experiments were conducted to study small scale infiltration processes beneath a smooth surface for homogeneous soil profiles for different soil types and initial moisture conditions (θ_i). Experimental studies were utilized to investigate the average θ_e above the advancing wetting front for different soil profiles during soil wetting (infiltration). Relationships between θ_e and θ_i were examined for three soil types with relationships then utilized for improved parameterization of a modified GA model to help account for some underlying assumptions of the model. Performance of the model at predicting wetting front movement was evaluated with the goal of improving the relationship between θ_i and soil-

water movement and investigate the performance of a GA model at predicting wetting front movement across changing initial soil conditions following the improved, experimentally-based parameterization.

The third chapter of this thesis introduces a new method for packing soil in laboratory scale soil boxes for experimental studies investigating overland flow-infiltration processes. The goal of the new method is to allow for the subsequent packing of soil profiles with identical, complex surface microtopography with uniform properties throughout the soil profiles. Accomplishing these feats would greatly enhance the capabilities of laboratory soil box experiments, particularly on overland flow generation processes, by allowing for an evaluation of the effect of identical, subsequent surface microtopography on various hydrologic processes.

The forth chapter of this thesis investigates the effect of microtopography on infiltration and soil-water movement processes at two different laboratory scales. The soil packing method in Chapter 3 was utilized to replicate soil surfaces utilizing two different soil conditions. Moisture sensors were installed in the soil profiles to evaluate infiltration/soil-water movement processes as related to surface microtopography under simulated rainfall. In addition, a small soil box was utilized to conduct small scale studies on the effect of microtopography on infiltration and soil-water movement processes. For small scale studies, the visible wetting front within the soil profile pertaining to different microtopographic features was observed and utilized for analysis by cutting the soil profile following simulated rainfall.

The purpose to this organization is that all studies described in chapters, though somewhat separate in their individual scopes, are combined to offer valuable insight into

infiltration processes for a range of soil and surface microtopographic conditions and additionally spur future research on this extremely important topic.

The experimental work presented in this thesis was conducted in the NDSU Civil Engineering Department Overland Flow Laboratory (OFL). The OFL was established in 2008 with the general purpose/function of studying a wide array of overland flow processes including overland flow generation (e.g., surface ponding, triggering, and connectivity), infiltration, and soil-water movement. The unique aspect of this laboratory is the capability of investigating the effect of surface topography (specifically microtopography) on each of these processes at varying spatial scales.

The OFL has a variety of unique equipment. Notably, the laboratory has a rainfall simulator (Meyer and Harmon 1979; Meyer 1994) and an instantaneous-profile laser scanner (Huang and Bradford 1990; Darboux and Huang 2003). The rainfall simulator allows for the replication of natural rainfall conditions across a surface area of 1.5 x 4.5 m. The instantaneous-profile laser scanner allows for obtaining high resolution surface DEM data with horizontal and vertical resolutions of 0.98 and 0.50 mm, respectively. Additional laboratory instruments and facilities include soil boxes for packing soil, moisture sensors, and a frame enabling the replication of complex surface microtopography. Various computer software programs and tools are also available in the lab [e.g., Hydrol-Inf (Chu and Mariño 2006) and a Puddle Delineation Program (Chu et al. 2010)] and are utilized for both modeling purposes and determining various surface characteristics (e.g., maximum depression storage). The major equipment and computer software programs utilized in this study will be introduced and described in greater detail throughout this thesis.

CHAPTER 2. ESTIMATION OF EFFECTIVE WATER CONTENT USING LABORATORY EXPERIMENTAL DATA FOR IMPROVING GREEN-AMPT WETTING FRONT MODELING

2.1 ABSTRACT

The Green-Ampt (GA) model has been widely used for modeling infiltration/runoff processes. In applications of the GA method, improved estimation of the GA parameters [e.g., effective water content (θ_e), capillary suction head (H_s), and effective hydraulic conductivity (K_e)] is critical to model performance for changing initial soil conditions. In this study, laboratory soil box experiments were utilized for the improved parameterization of GA effective saturated moisture content (θ_e). A mass-balance approach was used to determine average θ_e above observed wetting fronts for three soil types [loamy sand (LS), silty clay loam (SCL), and silty clay (SC)] and five initial moisture contents (θ_i). Linear relationships were determined for θ_e versus θ_i. The slopes of linear θ_e-θ_i regression for the LS, SCL, and SC were -0.55, -0.66, and -0.69, respectively. These regression results were incorporated into the modified GA modeling (Case 1) conducted utilizing a Windows-based software package Hydrol-Inf. One additional modeling case (Case 2) utilizing a constant average field saturation value for each soil type was also examined and evaluated against Case 1. The modeled and observed wetting fronts were compared. The experimental method of estimating GA θ_e provided very good agreement between the modeled and observed wetting fronts and improved the performance of the modified GA model at predicting wetting front movement for three soil types and initial moisture conditions (i.e., different θ_i and soil textures). This study provides a method for improved

GA modeling with potential implications towards future incorporation into more complex infiltration modeling.

2.2 INTRODUCTION AND LITERATURE REVIEW

Infiltration is one of the first hydrologic processes to occur following the commencement of a rainfall event and is classified as one of the primary abstractions from rainfall (Haggard et al. 2005). Infiltration processes are affected by soil (e.g., soil texture, bulk density, and moisture condition), rainfall, microtopography, and other conditions. Accurately representing infiltration processes in modeling is extremely important for predicting water movement in soil as well as for partitioning rainfall between infiltration and surface runoff. The wetting front describes the leading edge of soil wetting as percolating water moves through the vadose zone. Characterization of this critical front and the moisture distribution above it is required for better understanding infiltration processes. Efforts to accurately simulate infiltration processes have been extensive and include a number of empirical, semi-empirical, and physically-based models. Some milestone historical efforts include the Green-Ampt (GA) model (Green and Ampt 1911), Richards equation (Richards 1931), and Philips model (Philips 1955, 1957a,b). The Green-Ampt (GA) model (Green and Ampt 1911) was an early effort that has proven useful when appropriate parameter values are used. Therefore, parameter selection is important for a successful application to actual infiltration processes under varying soil and rainfall conditions.

The physically based GA model has been widely used for infiltration modeling and provides a well accepted, simplified representation of the infiltration process (Chu and Mariño 2005). The major assumptions in the GA model include piston flow, homogeneous

soil, uniform initial soil moisture distribution, and constant surface ponding. Modifications to the traditional GA model, however, have led to many successful applications for more complex situations including layered (non-uniform) soils, steady and unsteady rainfall, ponding and non-ponding conditions, and variably distributed initial water contents.

Childs and Bybordi (1969) and Bouwer (1969) applied the GA model to non-uniform soil profiles by partitioning the soil column into individual layers with dissimilar soil properties. Mein and Larson (1973) extended the traditional GA model and developed a two-stage model, which considered ponding time for infiltration in homogeneous soil under steady rainfall with Chu (1978) further modifying the GA model to handle infiltration under unsteady rainfall conditions. Beven (1984) developed a modified GA model for non-uniform soils under unsteady rainfall with the primary difference compared with earlier methods being that the soil profile was treated as continuous with an exponential function to describe saturated hydraulic conductivity with depth. Chu and Mariño (2005) developed a modified GA model for simulating infiltration into a layered soil profile of arbitrary initial moisture distributions under complex rainfall patterns and Loaiciga and Huang (2007) who presented a modified version of the GA model which considered ponding depth and time during different stages of the infiltration process. Liu et al. (2008) developed a modified version of the GA model capable of handling infiltration into non-uniform soils under unsteady rainfall. Ma et al. (2010) proved the effectiveness of a modified GA model by modeling infiltration into a long, layered soil column and determining it to be more accurate when compared to both Hydrus-1D and the traditional GA model. In one of the most recent examples, Kacimov et al. (2010) developed a GA model for a special layered soil profile case of a fine soil overlying a coarser soil.

One of the major aforementioned assumptions of GA infiltration is that of the nature of the wetting front (i.e., "sharp" piston flow). For a GA type model capable of simulating infiltration into a uniform soil layer and determining ponding status under rainfall, until surface ponding is achieved, the wetting front as described by the model will move as a fully saturated front controlled by the water storage deficit in the soil [i.e., saturated moisture content (θ_s) - initial moisture content (θ_i)] and rainfall intensity (r). In reality, however, the moisture distribution above the wetting front is often non-uniform. Descriptively, five soil moisture zones have been identified beneath a ponded soil surface and above the advancing wetting front. They include the saturation, transition, transmission, and wetting zones, and the wetting front (Bodman and Colman 1944; Williams et al. 1998). Beneath the wetting front, which represents a sharp change in volumetric moisture content (θ), very little change from θ_i is evident. For a non-ponding condition, the primary difference in the configuration of these zones can be the lack of a saturation zone. However, the entire wetted moisture profile will differ from that beneath a ponded surface. During soil wetting, the depth and θ within each of these zones change with time, but relative θ between them will remain fairly constant. A close approach of θ to saturation likely will occur near the surface under a ponded surface condition.

Therefore, before surface ponding is achieved, infiltration and soil-water movement may not necessarily agree with the underlying assumption of full saturation in the GA model. Due to the influence of entrapped air (Fayer and Hillel 1986; Faybishenko 1995; Hammecker et al. 2005) and non-uniform moisture distribution, the wetted soil may not be fully saturated and discrepancies may be present between the actual and GA modeled processes. Especially for wetting front movement, unless an estimated or effective water

content (θ_e) is used in place of θ_s, which accounts for the deviation of the actual soil-water movement from that described by the GA model, wetting front movement may not be accurately simulated by a GA model.

Ma et al. (2010) compared infiltration characteristics through a single layered soil column under a ponded surface to a modified GA model by introducing a saturation parameter based on the ratio of the average measured moisture content in the column in the soil profile to θ_s. In applying this ratio to θ_s and the saturated hydraulic conductivity (K_s), effective values of these two parameters were obtained, which, when applied in the model, achieved good agreement between the simulated and actual wetting front movement.

In this study, a series of laboratory infiltration experiments were conducted and utilized to better select parameter values for the modified GA model in the Hydrol-Inf software (Chu and Mariño 2006). The specific objectives of this study were to: 1) use a mass-balance approach and observed wetting front data from laboratory experiments to determine the average effective moisture contents θ_e in the wetted profiles for application of the Hydrol-Inf modeling; 2) investigate the relationship between this mass-balance based θ_e and initial soil-water content θ_i for three different soil types; and 3) evaluate the effectiveness of the θ_e parameter in the GA modeling and simulation of wetting front as a function of θ_i by comparing with the observed data. The goal is to show that using the data from laboratory experiments, the GA model can be parameterized, which is able to provide improved modeling of wetting front movement for varying soil types and initial moisture conditions.

2.3 METHODOLOGY

2.3.1 Soil Box

For laboratory infiltration experiments, soil was packed into a specially designed soil box. The soil box was constructed of clear plexiglass with the total outside dimensions of 62, 21, and 30 cm long, wide, and tall, respectively. Within the outside perimeter, the box was separated into three equally sized compartments (20 x 20 x 30 cm) using two plexiglass dividers, thereby enabling the packing of three separate soil profiles for each experiment. The bottom of each compartment also consisted of plexiglass sheets with nine 1.3 cm diameter holes evenly spaced in a grid pattern and covered with 2 mm screen to allow for unrestricted air movement through the bottom of the profile.

2.3.2 Soil and Soil Packing

Three soil types were used for laboratory experiments: Lohnes (Sandy, mixed, frigid Entic Hapludoll) loamy sand (LS), Bearden (Fine-silty, mixed, superactive, frigid Aeric Calciaquoll) silty clay loam (SCL), and Fargo (Fine, smectitic, frigid typic epiaquerts) silty clay (SC), with particle makeup and densities (ρ_p) shown in Table 2.1. To process the soils for experiments, the LS and SCL were air-dried and sieved through a 2 mm screen to remove large soil aggregates. The SC, due to difficulties as attributed to the high clay content, was air-dried and then processed using a soil processing machine, which used rotating metal "fingers" to break apart soil clods and sieve out large aggregates and roots/grass. All ρ_p values were determined for post-processed soils.

Table 2.1 Basic Soil Properties and Parameters

Soil	Sand (%)	Silt (%)	Clay (%)	Particle Density ρ_p (kg/m^3)	Bulk Density ρ_b (kg/m^3)	Porosity n
Loamy Sand	80.3	14.6	5.1	2,630	1,400	0.468
Silty Clay Loam	11.1	60.1	28.8	2,560	1,070	0.582
Silty Clay	4.2	46.7	49.1	2,580	1,000	0.612

Soil was packed into each compartment in 5 cm layers to a final depth of 27.5 cm. For packing, predetermined volumes of water were added to the soils and uniformly mixed. For each packing layer, the mass of soil was determined based on the predetermined target bulk density (ρ_b) (Table 2.1), initial gravimetric moisture content (θ_g), and the volume of each layer. For each packed profile, soil samples were taken and dried for 24 hrs at 105° C to determine actual θ_g. Precise ρ_b and θ_i (based on θ_g and ρ_b) values were then determined for each soil profile. The range of θ_i for each soil was limited at the upper end by the maximum $\theta_{i,max,}$ for which the wetting front movement could still be visually observed and for the minimum $\theta_{i,min}$ by wetting front stability, as very dry soil produced unstable wetting front movement (Rooij 2000).

2.3.3 Norton-style Rainfall Simulator

A Norton-style rainfall simulator was used for this study. It utilizes four oscillating VeeJet nozzles and has been proven to closely replicate natural rainfall characteristics including raindrop size, terminal velocity, energy, and spatial distribution (Meyer and Harmon 1979; Meyer 1994). At the design height of 2.44 m above the soil surface, the simulator is capable of providing rainfall to a 1.5 x 4.5 m surface area with programmable rainfall intensities ranging from 0.97 to 10.42 cm/hr by controlling the nozzle sweep frequency. Rainfall intensities were chosen based on soil types in an effort to achieve surface ponding for each soil type within a reasonable time period ($\approx$ 1 hr) and before the wetting front reached the bottom of the soil box. The average rainfall intensities used for the experiments were 3.85 cm/hr for the SCL and SC soils and 6.26 cm/hr for the LS soil across the entire soil box surface area. Calibration of the rainfall simulator was conducted and the rainfall intensity for each 20 x 20 cm surface was determined.

2.3.4 Laboratory Experiments and Data Processing

Laboratory experiments were conducted by simulating rainfall across homogeneous soil profiles packed using the aforementioned method for the three soil types with five θ_i values for each soil (total 15 experiments, Table 2.2). For each experiment, up to three separate soil profiles were packed in the individual soil box compartments. The observed surface ponding time (t_p) was recorded and used for mass-balance computation, calibration of model parameters, and evaluation of the simulated t_p across the full range of θ_i. The wetting front movement was recorded on two-minute intervals at two locations on opposite sides of each soil profile.

Following experiments, average effective water contents in the wetted profile were determined for each experimental profile based on overall mass balance as follows:

$$\theta_e=\theta_i+\frac{rt_w}{d_{wf}} \tag{2.1}$$

where r = rainfall intensity (cm/hr); t_w = time (hr); d_{wf} = wetting front depth at time t_w (cm); θ_i = initial water content (cm^3/cm^3); and θ_e = average effective water content (cm^3/cm^3). The values of θ_i, r, t_w, and d_{wf} for all experiments are shown in Table 2.2. Fig. 2.1 illustrates the methodology and shows the average equivalent θ_e GA parameter determined based on the actual wetting front depth and the mass-balance principle for utilization in this study. Two separate wetting fronts simulated by utilizing θ_s and θ_e in the GA model, and their comparisons with the actual wetting front are schematically shown in Fig. 2.1. Fig. 2.1 also shows the methodology behind θ_e determined and utilized in this study.

Table 2.2. 15 Experiments for the Three Soil Types

Exp.[a]	Initial Moisture Content θ_i (cm^3/cm^3)	Bulk Density ρ_b (kg/m^3)	Rainfall Intensity r (cm/hr)	t_p[b] (min.)	t_w[c] (min.)	d_{wf}[d] (cm)
LS1	0.067	1,390	6.36	N/A	44	19.55
LS2	0.074	1,400	6.36	N/A	44	19.95
LS3	0.082	1,400	6.13	46	44	20.80
LS4	0.093	1,410	6.29	40	40	20.70
LS5	0.109	1,400	6.29	26	24	14.35
SCL1	0.127	1,070	3.90	N/A	40	5.85
SCL2	0.180	1,090	3.90	26	26	4.80
SCL3	0.200	1,060	3.88	24	22	4.35
SCL4	0.236	1,080	3.88	16	14	3.65
SCL5	0.273	1,070	3.84	12	12	3.70
SC1	0.116	980	3.78	14	14	1.80
SC2	0.175	980	3.84	12	12	2.05
SC3	0.224	980	3.90	10	10	2.15
SC4	0.276	1,000	3.90	8	8	2.35
SC5	0.304	1,020	3.84	6	6	2.35

[a]LS is the loamy sand soil, SCL is the silty clay loam soil, SC is the silty clay soil, and 1 - 5 describe the five different experiments using each soil
[b]t_p is the observed time to surface ponding
[c]t_w is the time for the final wetting front depth used for mass balance analysis
[d]d_{wf} is the wetting front depth at t_w used for mass-balance

The t_w and the corresponding d_{wf} values were chosen for each experiment at or slightly before t_p. This allowed for a comparison of wetting front movement for the longest time period possible before surface ponding for each soil type. For the case of the two driest LS experiments and the driest SCL experiment, however, surface ponding was not achieved within the duration of the experiments and therefore t_w and d_{wf} were taken near the end of the experimental time to allow for the comparison of as much wetting front data as feasible. The average effective water content of the wetted zone was utilized for the GA modeling in Hydrol-Inf and will be further discussed later.

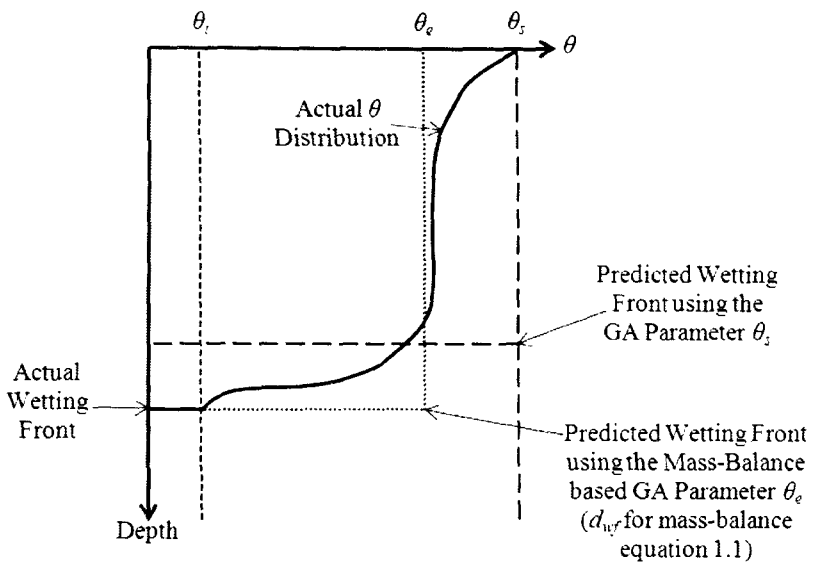

Figure 2.1. Actual moisture distribution during soil wetting and the Green-Ampt effective wetted zone. Note: θ_i is the initial moisture content; θ_e is the average effective moisture content based on the mass-balance relationship; θ_s is the saturated moisture content; θ is the volumetric moisture content.

Regression analysis was then performed to determine the relationship between θ_e and θ_i for all three soil types. Additionally, each value of θ_e was converted to soil saturation (S) for all the corresponding values of θ_i by:

$$S = \frac{\theta_e}{\theta_s} \times 100 \tag{2.2}$$

where θ_s = saturated water content (cm^3/cm^3) (equal to n); and S = saturation (%).

2.3.5 Introduction to Hydrol-Inf

In this study, the Windows-based software, Hydrol-Inf (Chu and Mariño 2006) was used for simulating infiltration and soil-water flow. Chu and Mariño (2005) developed a modified GA model capable of simulating infiltration into heterogeneous soil profiles of arbitrary initial moisture distributions under unsteady rainfall conditions. The model is able to handle the shift between ponding and non-ponding conditions as well as predict the current ponding status. This is compared with the original GA model for which both a

homogeneous soil profile and constant surface ponding were assumed, both of which deviate significantly from real conditions for almost all cases. The model described by Chu and Mariño (2005) was also further extended to continuously simulate infiltration and surface runoff under any complex rainfall patterns (multiple rainfall events) that may include both wet and dry time periods, and incorporated into the Hydrol-Inf software (Chu and Mariño 2006). Hydrol-Inf provides all details on infiltration, rainfall excess, surface ponding conditions, soil-water flow along the profile, soil-water content and distribution over the entire simulation time period. The modified GA model in Hydrol-Inf was chosen for simulating infiltration and soil water flow in this study.

2.3.6 Determination of GA Modeling Parameters

In utilizing the GA method for infiltration modeling, one of the major advantages is the simplicity of the model. However, knowledge of soil properties including saturated water content (θ_s), capillary suction head (H_s), and hydraulic conductivity (K) is required for the determination of accurate modeling parameter selection (Bouwer 1969). Accurate estimation of such soil parameters for the GA method has been an issue which has received considerable attention.

In this study, the effective water content (θ_e) was determined based on the observed wetting front data and mass-balance [Eq. (2.1)]. Regression equations were then fitted for θ_e and θ_i for each soil type and θ_i. The actual values of θ_e used in Hydrol-Inf in place of θ_s, however, were not values determined directly from Eq. (2.1) for each θ_i. The θ_e values used in Hydrol-Inf were instead calculated using the fitted regression equations as a function of each experimental θ_i for all three soil types (Case 1). One additional simplified modeling case (Case 2) using constant values of θ_e was also used for comparison purposes to

highlight the improvements gained in modeling of the new θ_i-dependent θ_e parameter and is further discussed in the section of Modeling and Evaluation Procedure.

The estimation of H_s and K was accomplished using a combination of experimental and theoretical methods [RETC program (van Genuchten et al. 1991)]. Van Genuchten et al. (1991) developed the Windows-based RETC software based on the method described by van Genuchten (1980) as a tool to predict both water retention and conductivity relationships for soil using a variety of methods. RETC incorporates several widely-used soil-water retention models (Brooks and Corey 1964; van Genuchten 1980; Kosugi 1996) and conductivity models (Burdine 1953; Mualem 1976).

2.3.6.1 GA Capillary Suction (H_s)

Many methods have been developed for estimating the GA parameter H_s, which describes the average capillary suction at the advancing wetting front. The simplest and one of the most common methods is the use of average H_s values based on general soil properties (e.g., texture, ρ_b, organic matter, and K_s) (Rawls and Brakensiek 1982, 1983; Rawls et al. 1983a, 1983b; Van Mullen 1989). More complicated methods exist for directly estimating H_s based on the knowledge of experimentally or theoretically determined relationships between various soil properties including K, θ, capillary pressure (P_c), and diffusivity (D) (Bouwer 1966; Mein and Larson 1971, 1973; Neuman 1976; Panikar and Nanjappa 1977; Slack and Larson 1981).

In addition to the direct methods, indirect methods also have been developed for estimating H_s based on soil-water retention characteristics. One of the most common and well accepted methods utilizes the soil-water retention model proposed by Brooks and

Corey (B & C) (1964), from which the air entry pressure of the soil (P_a) can be determined and used to estimate H_s. The B & C model can be described as:

$$S_f = \frac{\theta - \theta_r}{\theta_s - \theta_r} = \left(\frac{P_a}{P_c}\right)^{\lambda} = \left(\frac{1}{\alpha' P_c}\right)^{\lambda} \qquad P_c \geq P_a, \alpha' P_c > 1 \tag{2.3}$$

where S_f = effective saturation; θ_r = residual water content (cm^3/cm^3); P_c = capillary pressure (cm); P_a = air entry pressure (cm); λ = B & C coefficient; and α' = reciprocal of P_a (1/cm). Based on the value of P_a determined using the B & C model, various relationships have been proposed for relating this parameter to H_s (e.g., Brakensiek 1977) with one simple but well accepted method proposed by Bouwer (1969):

$$H_s = 0.5 \times P_a \tag{2.4}$$

The method used to determine H_s in this study was based on Eq. (2.4) with the value of P_a determined by using the B & C model in the RETC software. According to van Genuchten et al. (1991), the B & C model is well suited for sieved and repacked soils, which was the case in this study. Soil-water retention curves were first determined for matric potential from 0 to 1,500 kpa using the tempe cell, pressure cooker, and pressure plate methods. A fitted soil-water retention curve was then developed using the B & C model in the RETC software and P_a values for each soil were determined. The calculated H_s values were subsequently utilized directly in the Hydrol-Inf modeling.

2.3.6.2 GA Hydraulic Conductivity (K)

Under the fully-saturated condition, K is equal to its maximum (K_s). In reality, however, complete saturation of the entire wetted soil profile is uncommon. Due to the influence of entrapped air and many other factors, K is generally less than K_s and an effective hydraulic conductivity value (K_e) is commonly used in the GA models. One

simple but well accepted method for determining the relationship between K_e and K_s was proposed by Bouwer (1969):

$$K_e = 0.5 \times K_s \tag{2.5}$$

In this study, K_s was experimentally determined using the constant head permeameter method for each soil type and an initial estimate of K_e was then calculated using Eq. (2.5). K values were also verified using a mini disk infiltrometer (Zhang 1997). The K values from the infiltrometer were experimentally determined for θ_i values approximately in the middle of the ranges of experimental θ_i values for all soil types. Due to increased precision and consistency associated with the falling head permeameter method, K_s values determined using this method were utilized for this study.

Initial estimated K_e values were then calibrated by using the experimental data. GA H_s describes the average suction head at the advancing wetting front, whereas GA K_e describes the average hydraulic conductivity in the entire wetted profile above the wetting front. Therefore, H_s will be affected minimally by changing surface conditions with progression of the experiments; whereas K_e can be strongly influenced by any changes in surface conditions. Thus, adjusting K is the most effective way for model calibration. K also is the GA parameter exerting the most control over ponding time. For each soil type, one calibrated K_e value was chosen to best fit the entire range of t_p for all θ_i values (different experiments) and utilized for modeling in Hydrol-Inf. K_e was adjusted using a trial and error method to obtain the best possible agreement between the model simulated and observed t_p for each soil type across all θ_i values.

2.3.7 Modeling and Evaluation Procedure

After selecting all model parameters, GA modeling was conducted utilizing Hydrol-Inf and the simulated wetting fronts were compared with the observed ones for all experiments involving the three soil types and five initial water contents for each soil. For comparisons, the root mean square errors (*RMSE*) of the modeled from observed wetting front depths were calculated across the entirety of all experiments for two minute intervals (the same as the observed wetting front interval). The relative errors between the simulated and observed were computed for all experiments (five experiments per soil type, Table 2.2).

The two modeling cases were compared with the observed wetting front movements. Both cases utilized the same values of H_s and K_e, but involved the use of different values of θ_e in place of the GA parameter θ_s. For Case 1, as aforementioned, the values of θ_e (θ_{e1}) calculated by utilizing the θ_i-θ_e regression equations for each soil type were used. In effect, unique, fitted values of θ_e which were directly related to each θ_i for each soil type were used in the modeling. For Case 2, however, similar to many other GA-type modeling applications, a constant value of θ_e (θ_{e2}) determined as an average percent of the total porosity n was used for each soil type over the entire range of θ_i values. These percentages reflect average field saturation values typical of soils and are commonly used in infiltration modeling to account for the effects of entrapped air and other unknown factors if soil porosity (n) is known. These percentages were chosen as $0.8n$ for the LS and $0.9n$ for the SCL and SC based on Slack et al. (1981) and Wilson et al. (1981) who stated that entrapped air generally accounts for 10 - 20% of the total porosity in field saturated

soils, with the percentage highest for coarser textured soils. Unlike Case 1, θ_e values utilized in Case 2 were constant across the entire ranges of θ_i for all soil types.

The purpose of these two cases was to highlight the advantages of using θ_e values which are directly related to θ_i in place of the GA θ_s to help account for the effect of θ_i on soil-water movement in order to improve the simulation of wetting front movement (Case 1). In addition, the two cases were utilized to show the disadvantages of using constant θ_e values in place of the GA θ_s which do not reflect the effect of changing θ_i (Case 2). Referring to the aforementioned K_e calibration process, separate values were calibrated for Case 1 (K_{e1}) and Case 2 (K_{e2}). For the SCL and SC, however, the same calibrated K_e values were used as they provided the best fit for both cases.

2.4 RESULTS AND DISCUSSION

2.4.1 Average Effective Water Content and Saturation

The experimentally based θ_e values for corresponding values of θ_i as determined using the mass-balance method for all soil types are shown in column one in Table 2.3, with experimental t_w, d_{wf}, r, and θ_i values (Table 2.2) used in Eq. (2.1) for the calculation of θ_e as aforementioned. The relationships of θ_e and θ_i determined for the three soil types were well fit by linear regression equations (Fig. 2.2) with R^2 values of 0.92, 0.95, and 0.98 for the LS, SCL, and SC, respectively. For all three soils, θ_e decreased with increasing θ_i. The slopes of the regression lines were -0.55, -0.66, and -0.69 for the LS, SCL, and SC, respectively (Fig. 2.2), which shows a stronger negative correlation between θ_e and θ_i with increasingly finer soil texture. For the LS, a relatively narrow range of θ_i (Fig. 2.2) was possible for experiments as attributed to the ability to observe the wetting front while for the SC, the very low K value led to rather short experimental durations due to early surface

ponding. The consistency of these relationships of mass-balance determined θ_e and θ_i for all soil types, however, was very interesting and clearly expressed the critical role of initial moisture content played in soil-water movement characteristics.

Table 2.3. Effective Moisture Content, Percent Saturation, and GA Modeling Effective Moisture Content for Cases 1 and 2 for all Experiments

Exp.[a]	θ_e[b] (cm^3/cm^3)	Percent Saturation S (%)	Fitted Case 1 GA θ_{e1} (cm^3/cm^3)	Case 2 GA θ_{e2} (cm^3/cm^3)
LS1	0.306	65.04	0.308	0.370
LS2	0.308	65.53	0.304	0.370
LS3	0.298	63.44	0.300	0.370
LS4	0.296	63.93	0.294	0.370
LS5	0.284	61.48	0.285	0.370
SCL1	0.572	98.21	0.570	0.520
SCL2	0.532	91.42	0.535	0.520
SCL3	0.527	90.61	0.521	0.520
SCL4	0.484	83.22	0.497	0.520
SCL5	0.481	82.56	0.473	0.520
SC1	0.606	99.02	0.600	0.550
SC2	0.549	89.75	0.560	0.550
SC3	0.526	85.96	0.526	0.550
SC4	0.497	81.23	0.490	0.550
SC5	0.467	76.37	0.470	0.550

[a]LS is the loamy sand soil, SCL is the silty clay loam soil, SC is the silty clay soil, and 1 - 5 describe the five different experiments using each soil
[b]θ_e is the mass-balance based effective moisture content

This relationship of θ_e with θ_i makes sense. As discussed earlier, K has a positive relationship with θ_i while H_s has a negative/inverse relationship with θ_i. As a result, for all soil types, lower θ_i will result in lower K and higher H_s values, while the opposite will hold true for higher θ_i. Therefore, for higher θ_i, water may be more easily conducted through the higher percentage of water filled pores while experiencing less capillary suction drawing water into finer pores (faster movement of the wetting front). Conversely, for lower θ_i, water will generally experience higher capillary suction and lower hydraulic conductivity

(slower movement of the wetting front), potentially drawing water into finer pores. Using the values of θ_c determined by mass balance analysis (Table 2.3), S values for each soil type were determined using Eq. (2.2). S values are also listed in Table 2.3 and plotted in Fig. 2.2. The maximum values of S for the LS, SCL, and SC were equal to 65.0, 98.2, and 99.0%, and the average S values for all five experiments (different θ_i values) were 63.5, 89.2, and 86.4% for the LS, SCL, and SC, respectively. The average S values for the SCL and SC fit the average field saturated values ($0.8n$ to $0.9n$) described earlier. However, the S value for the LS was relatively low (Fig. 2.2a, Table 2.3). Low S values for the LS may possibly be reflective of very rapid wetting front movement and less complete wetting of the profile. El-Shafei and Al-Darby (1991) found in laboratory experiments utilizing a soil with a very high sand content that average S values throughout the transmission zone were within the suggested field saturation range of $0.8n$ to $0.9n$ (81.2%). However, this is not reflective of the average S above the furthest advancing wetting front, for which case S likely may have been considerably lower than 81.2% and similar to values observed for the LS in this study (i.e., average of 63.5%).

This point clearly illustrates the strong influence of soil textures on wetting front movement as well as the potential difficulties in accurately predicting the wetting front movement through different soil textures, particularly coarser textured soils, due to the vastly different water-movement characteristics. In coarser textured soils, the average S above the advancing wetting front may be considerably different from the average S throughout the transmission zone (i.e., largest wetting zone during soil wetting).

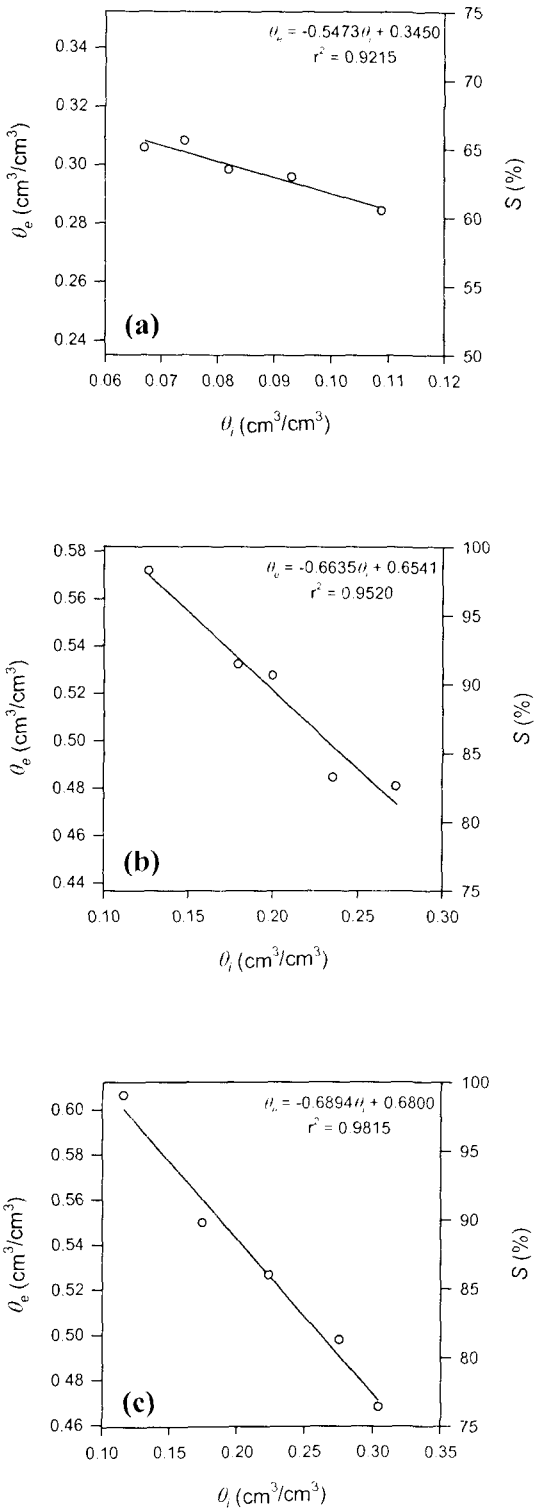

Figure 2.2. Relationships between initial water content θ_i and effective water content θ_e (or saturation S) for the three selected soil types. (a) Loamy Sand. (b) Silty Clay Loam. (c) Silty Clay.

2.4.2 GA Moisture Parameters

All moisture parameters (θ_i and θ_e) for the GA modeling were finalized for both Cases (1 and 2). The θ_i values utilized for modeling each laboratory soil profile were taken directly as the experimental θ_i determined for each profile (Table 2.2). For the effective water contents used in place of the GA parameter θ_s in the modeling for the two aforementioned cases (θ_{e1} and θ_{e2} for Cases 1 and 2), θ_{e1} values were determined using the regression equations for each soil type and each θ_i utilized in modeling (Fig. 2.2, Table 2.3). For θ_{e2} used in Case 2, constant relationships of $0.8n$ for the LS and $0.9n$ for the SCL and SC were utilized with θ_{e2} values used in the modeling equal to 0.37 for the LS, 0.52 for the SCL, and 0.55 for the SC (Table 2.3).

2.4.3 GA Capillary Suction Head

For the determination of the GA H_s in this study, the B & C method was used to fit soil-water retention data. The final fitted B & C modeling parameters and the respective P_a values for all soil types are shown in Table 2.4. The B & C θ_s values in Table 2.4 were those fitted to the experimental data, which may vary slightly from the corresponding n values (Table 2.1). The SCL had a slightly higher P_a value than that of the SC, which may possibly be related to the differences in average ρ_b values [1,070 and 1,000 kg/m^3 for the SCL and SC (Table 2.1)] as well as the types of clays present in the SCL and SC. After determining P_a values, H_s for each soil type for use in the modeling was calculated using Eq. (2.4), producing values of 6.31, 42.74, and 36.39 cm for the LS, SCL, and SC, respectively (Table 2.4).

Table 2.4. Soil Hydraulic Parameters

Soil[a]	α[b] (1/cm)	θ_s[c] (cm^3/cm^3)	θ_r[d] (cm^3/cm^3)	m[e]	R^2[f]	P_a[g] (cm)	H_s[h] (cm)	K_{e1}[i] (cm/hr)	K_{e2}[j] (cm/hr)
LS	0.07926	0.417	0.058	0.93287	0.999	12.62	6.31	4.8	4.4
SCL	0.01170	0.520	0.173	0.38316	0.998	85.47	42.74	0.35	0.35
SC	0.01374	0.536	0.106	0.15045	0.979	72.78	36.37	0.2	0.2

[a]LS is the loamy sand soil, SCL is the silty clay loam soil, and SC is the silty clay soil
[b]α' is the fitted B & C parameter (inverse of P_a)
[c]θ_s is the fitted B & C saturated water content
[d]θ_r is the fitted B & C residual water content
[e]m is the fitted B & C parameter
[f]R^2 is the fitted B & C coefficient of determination
[g]P_a is the fitted B & C air entry pressure
[h]H_s is the GA capillary suction head
[i]K_{e1} is the calibrated GA effective hydraulic conductivity for Case 1
[j]K_{e2} is the calibrated GA effective hydraulic conductivity for Case 2

H_s is dependent on θ_i; however, it is close to constant over a wide range of θ_i values, particularly for drier soil (θ_i < 30% of θ_s) (Mein and Farrel 1974). Panikar and Nanjappa (1977) showed that uniform values of H_s were present over a wide range of soil moisture conditions up to at least 50% of θ_s, after which H_s began to decrease markedly with increasing θ_i. Similarly, in infiltration modeling, Mein and Larson (1973) used constant H_s values for soil types over a wide range of θ_i. In this study, the maximum θ_i values utilized in the laboratory experiments were 23, 46, and 50% of θ_s for the LS, SCL, and SC, respectively. Thus, a constant H_s value was used for each soil type across all θ_i values.

2.4.4 GA Hydraulic Conductivity

Experimentally determined values of K_s were 57.63, 3.67, and 0.36 cm/hr for the LS, SCL, and SC, respectively. The values of K_s for all soil types were additionally verified using a Decagon Mini Disk Tension Infiltrometer (Pullman, Washington), producing approximate average K_s values of 50.0, 4.0, and 0.7 cm/hr for the LS, SCL, and SC, respectively. These values agreed fairly well with the constant head permeameter K_s values. The high K_s values associated with all soil types (particularly the LS) as compared with the

average field values for similarly textured soils may be attributed to soil processing and repacking characteristics.

K_e values were then determined as 28.82, 1.84, and 0.18 cm/hr for the LS, SCL, and SC, respectively, using Eq. (2.5). K_c values were next calibrated based on t_p values shown in Table 2.2. The GA modeling parameters described above [H_s, θ_i, and θ_e (θ_{e1} or θ_{e2})] are shown in Tables 2.2 and 2.3. K_c was uniquely calibrated for both Cases 1 and 2 (utilizing θ_{e1} and θ_{e2}), producing final calibrated values of K_{c1} and K_{c2} for Cases 1 and 2, respectively (Table 2.4). The same final calibrated K_c values were determined for Cases 1 and 2 for the SCL and SC [0.35 and 0.2 cm/hr for the SCL and SC, respectively (Table 2.4)]. For the LS, the calibrated K_c values were 4.8 and 4.4 cm/hr for Cases 1 and 2, respectively (Table 2.4).

For the calibrated K_c values used in this study, the SC showed very good agreement with Eq. (2.5) at estimating the GA parameter K_c. For the SCL and LS, however, significant differences were found between the calibrated K_c and the initial estimates of K_c. Calibrated K_c was determined as to 9.5% of K_s for the SCL and 8.3% and 7.6% of K_s for the LS for Cases 1 and 2. One possible reason may be attributed to the effect of simulated rainfall on soil surface conditions, particularly for the longer durations in the SCL and LS experiments. The calibrated K_c values, therefore, are average "lumped" K values, which take into account all additional experimental factors, similar to the experimentally determined θ_e values.

2.4.5 Wetting Front Movement

After determining all GA modeling parameters [i.e., θ_i, H_s, θ_e (θ_{e1} and θ_{e2} in Cases 1 and 2), and K_e (K_{e1} and K_{e2} in Cases 1 and 2)] as described above (Tables 2.2, 2.3, and 2.4), Hydrol-Inf was utilized for simulating infiltration, soil-water flow, and surface ponding

status. The simulated wetting fronts were then compared with the observed ones for Cases 1 and 2. The maximum *RMSE* values for the LS, SCL, and SC were 0.41, 0.30, and 0.11 cm for Case 1 and 3.94, 0.53, and 0.63 cm for Case 2, respectively, while the averages for the three soil types were 0.27, 0.23, and 0.09 cm for Case 1 and 3.39, 0.34, and 0.33 cm for Case 2, respectively (Table 2.5). Figs. 2.3-2.5 show the comparisons between the simulated and observed wetting fronts for the three soil types and five different θ_i for each soil type for Cases 1 and 2.

Table 2.5. Case 1 and 2 Root Mean Square Errors of Simulated from Observed Wetting Fronts, Simulated Ponding Times, and Relative Errors of Simulated from Observed Ponding Time

	Case 1			Case 2		
Exp.[a]	*RMSE* (cm)	$t_{p,sim}$[b] (min.)	t_p Relative Error[c] (%)	*RMSE* (cm)	$t_{p,sim}$[b] (min.)	t_p Relative Error[c] (%)
LS1	0.17	N/A	N/A	2.82	N/A	N/A
LS2	0.24	N/A	N/A	2.93	N/A	N/A
LS3	0.41	50	8.7	3.68	46	0
LS4	0.30	40	0	3.94	40	0
LS5	0.21	35	34.6	3.57	37	42.3
SCL1	0.12	N/A	N/A	0.28	N/A	N/A
SCL2	0.29	24	7.7	0.26	23	11.5
SCL3	0.22	22	8.3	0.22	22	8.3
SCL4	0.30	18	12.5	0.42	19	18.8
SCL5	0.21	14	16.7	0.53	17	41.7
SC1	0.11	16	14.3	0.24	15	7.1
SC2	0.08	13	8.3	0.07	12	0
SC3	0.09	10	0	0.17	10	0
SC4	0.08	7	12.5	0.56	9	12.5
SC5	0.09	6	0	0.63	8	33.3

[a]LS is the loamy sand soil, SCL is the silty clay soil, SC is the silty clay loam soil, and 1 - 5 describe the five different experiments using each soil

[b]$t_{p,sim}$ is the models ponding time

[c]t_p Relative Error is the relative error for the modeled ponding times from the actual experimental ponding times

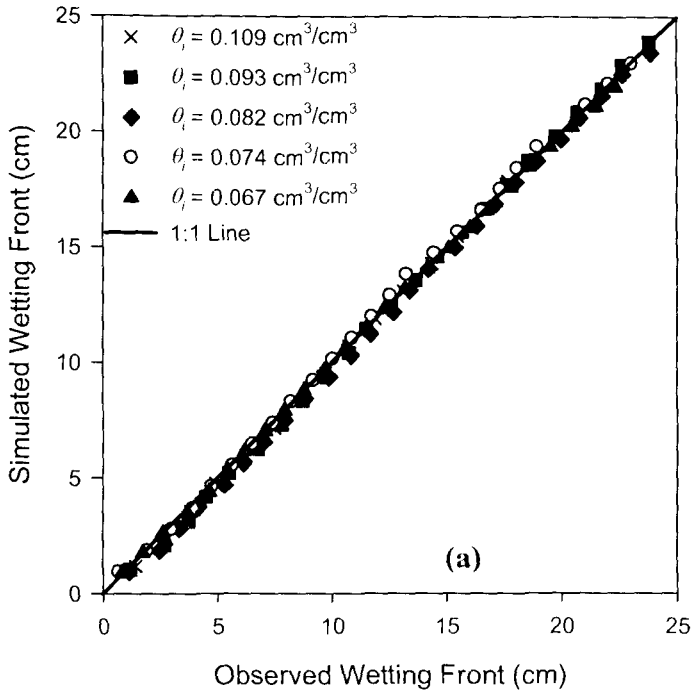

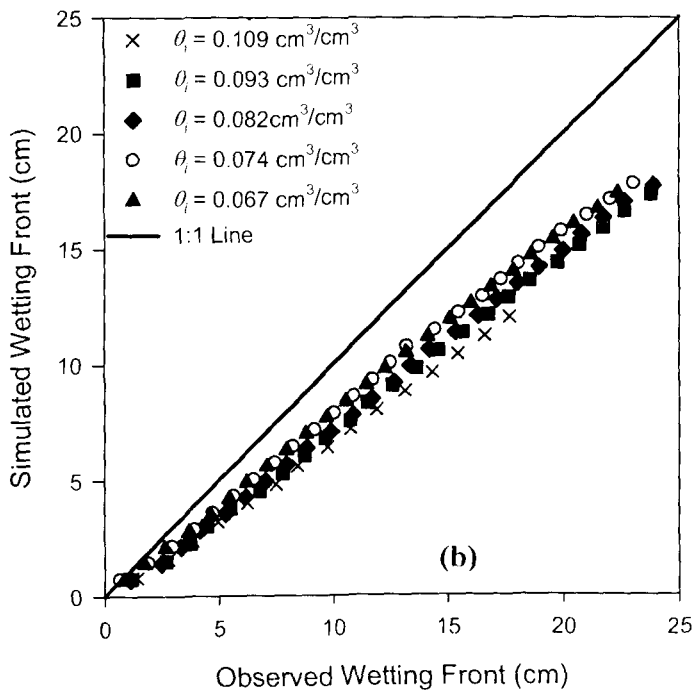

Figure 2.3. Comparison between the simulated and observed wetting front depths in the loamy sand soil for Cases 1 and 2. (a) Case 1. (b) Case 2.

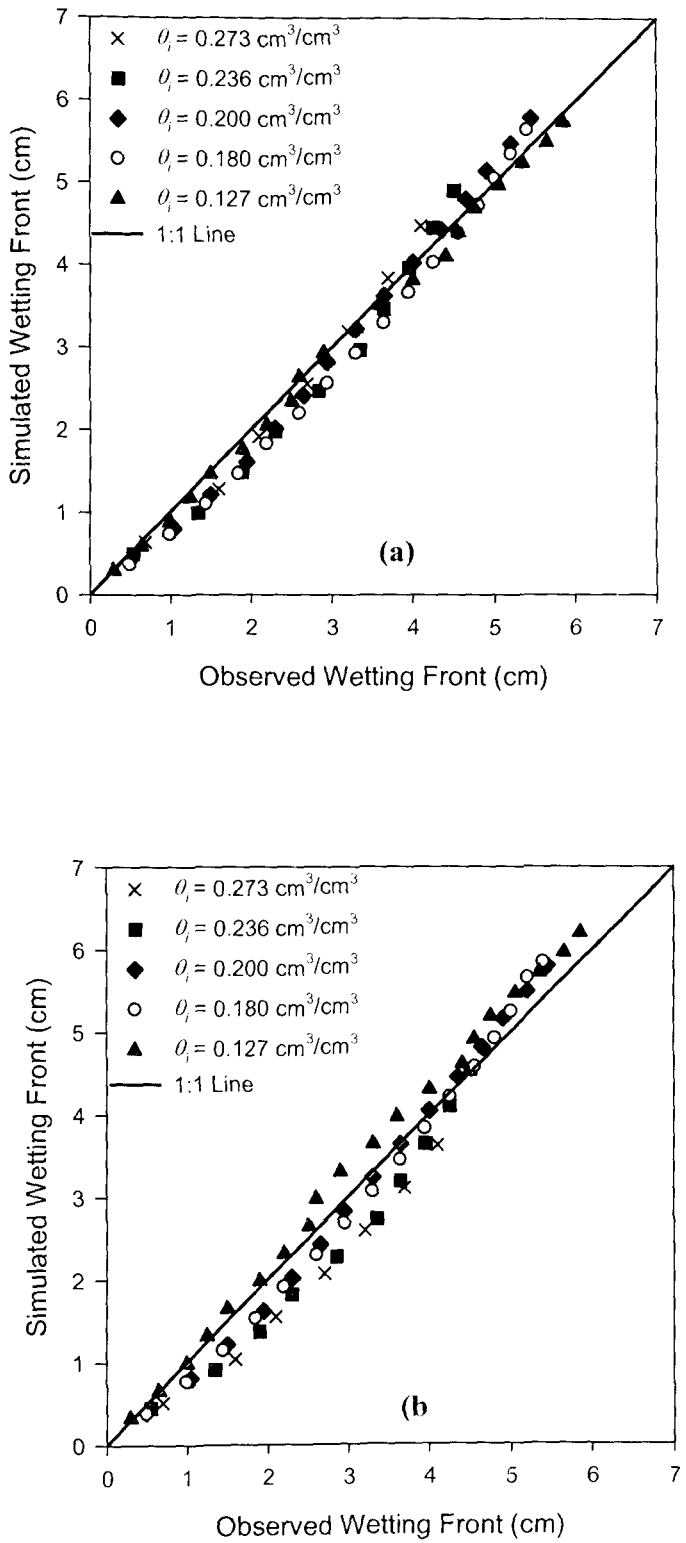

Figure 2.4. Comparison between the simulated and observed wetting front depths in the silty clay loam soil for Cases 1 and 2. (a) Case 1. (b) Case 2.

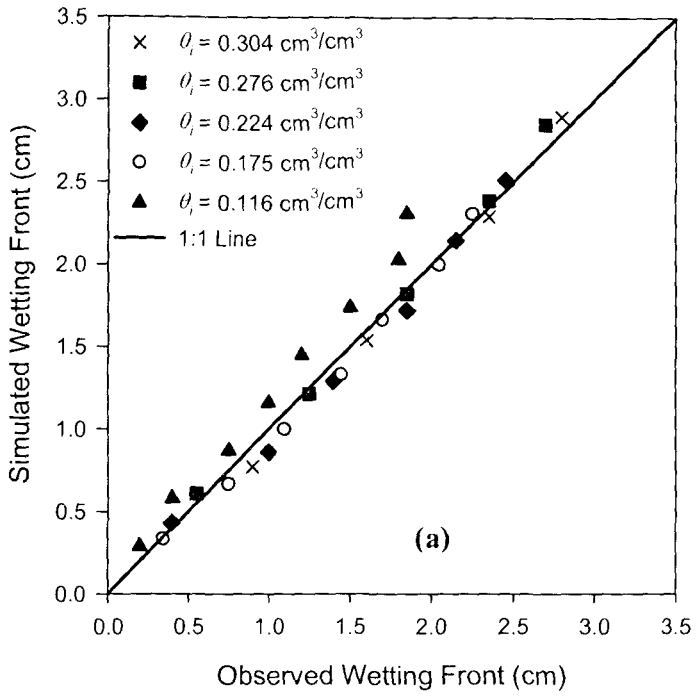

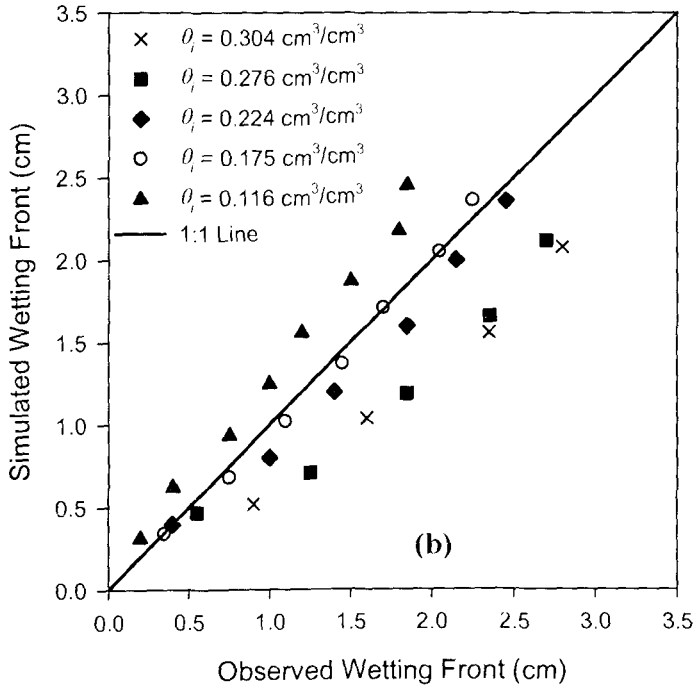

Figure 2.5. Comparison between the simulated and observed wetting front depths in the silty clay soil for Cases 1 and 2. (a) Case 1. (b) Case 2.

These modeling results clearly show that for Case 1 the GA model yielded accurately simulated wetting front movement over the full range of θ_i values for all soil types as attributed to the utilization of the mass-balance based θ_{c1} parameters. For Case 2 with constant θ_{c2} values, the model performed adequately for wetting front prediction for the SCL and SC, however not nearly as well as Case 1. For the LS, however, significant differences can be observed between Cases 1 and 2, which highlights the improvement achieved from using the proposed method in Case 1.

For both the SCL and SC, wetting front movement was described equally as well by the criteria in Case 2 as Case 1 for one SC experiment (Exp. SC2, Table 2.2) and two SCL experiments (Exp. SCL2 and SCL3, Table 2.2), as indicated by similar *RMSE* values for Cases 1 and 2 (Table 2.5). This can also be observed in a very good fit to the 1:1 line for Case 2 in Figs. 2.4 and 2.5 for the aforementioned experiments. These agreements between Cases 1 and 2 occurred where the constant GA parameter θ_{c2} used in the Case 2 modeling (Table 2.3) intersected the θ_c-θ_i regression lines (Fig. 2.2) used for describing θ_{c1} for Case 1. For experiments with progressively more extreme θ_i values (further distance away) from the intersection where θ_c values for Cases 1 and 2 matched closely, Case 2 parameters performed progressively worse in the modeling while the Case 1 model performed consistently over the entire range of θ_i. For the LS, however, modeling for Case 2 provided very poor simulated wetting fronts compared with those observed, with the discrepancy larger with increasing θ_i (Fig. 2.3b). This may be attributed to the large discrepancy between the mass-balance based θ_{c1} and the constant θ_{c2} as aforementioned, and the increase in the discrepancy with increasing θ_i.

For the LS in both Cases 1 and 2, the errors between the modeled and observed wetting fronts were rather uniformly distributed throughout the duration of the experiment (Fig. 2.3). A similar trend was observed for the SC, for which over/under-prediction of wetting front by the model was consistent for the duration of the experiments, with discrepancies much more pronounced for Case 2 (Fig. 2.5b). For the SCL, however, a different trend was noticed, especially for Case 2 (Fig. 2.4b). The model under-predicted wetting front movement earlier on in the experiments (especially for progressively lower θ_i values) and then gradually began over-predicting wetting front movement at later durations in the experiments. Case 1 had a similar trend (Fig. 2.4a), but discrepancies were much less and overall better agreement was achieved.

In a GA model, as described earlier, wetting front movement is a function of the soil-water deficit (θ_s - θ_i). Therefore, if the observed wetting front movement deviates significantly from a constant rate (i.e., non-linear movement) due to specific soil properties before surface ponding occurs, the model may not accurately predict wetting front movement for this situation. In the case of non-linear wetting front movement, the utilization of the mass-balance based method described in this study for fitting θ_e to the observed experimental wetting front data may only produce good agreement between the modeled and observed wetting fronts close to the time where the t_w-d_{wf} relationship was chosen for use in Eq. (2.1) for determining θ_e values. However, the fit before this time may not be good, and the simulated and observed wetting front movement may closely coincide only around the time of surface ponding where the utilized t_w-d_{wf} relationship was chosen. In this study, wetting front movement was simulated most accurately for the coarsest textured soil (LS) where the wetting front movement was most uniform. The model was

also capable of describing the two finer textured soils used in this study very well (SCL and SC).

The overall results from the GA modeling show that the Case 1 model more accurately simulated wetting front movement than the Case 2 model did, especially for the LS soil. The new GA parameterization method based on the experimental wetting front data performed very well. Using the fitted GA θ_{e1} parameter based on the mass-balance relationships improved modeling accuracy. The model simulated wetting front movement over the entire range of θ_i values. Case 2 performed adequately for the SC and SCL, but poorly for the LS. It may be possible, however, to perform one laboratory soil box experiment for one θ_i for each soil type, which could produce a θ_e value reflective of the average θ_e values across a range of θ_i (similar to Case 1 except constant values).

Additionally, use of the relationship of $0.8n$ to $0.9n$ for the GA θ_e may result in accurate simulation of wetting front movement in fine textured soils, but may grossly under-predict wetting front movement in coarse textured soils. For the LS, an average relationship of $0.65n$ would have provided an overall better simulation of wetting front for Case 2. In addition, ponding time (discussed in the next section) may have also contributed to the fit between the simulated and observed wetting fronts. Particularly for the SCL (i.e., Exp. SCL2 and SCL3), the under-estimation of t_p as simulated by the model from experimental t_p may have resulted in slowed modeled wetting front movement after ponding status was achieved in the model. As shown in Fig. 2.4a for Exp. SCL2 and SCL3, slower simulated wetting front movement near the end of the time period resulted in a closer fit to the 1:1 line. Therefore, the fit between the simulated and observed wetting fronts would have been worse near the end of the experiment durations and the subsequent

RMSE values would have been higher, had the model not under-predicted the ponding time for Exp. SCL2 and SCL3 near the end.

2.4.6 Ponding Time

The observed ponding times ranged from 26 to 46 min for the LS (Exp LS1 - LS5), from 12 to 26 min for the SCL (Exp SCL1 - SCL5), and from 6 to 14 min for the SC (SC1 – SC5) (Table 2.2). Note that the experimental ponding times t_p for three experiments (Exp LS1, LS2, and SCL1) are not available. For each soil type, it took longer time for the soil to reach the ponding status for drier soil conditions (lower initial water content) (Table 2.2).

Comparisons of the observed with modeled ponding times are shown in Table 2.5 with experimental ones used for comparisons found in Table 2.2. Overall, the Case 1 model performed slightly better, particularly at predicting t_p across the more extreme ranges of θ_i for the SCL. In Case 1, the relative errors between simulated and observed t_p values for Exp. SCL1 and SCL 5 were 7.7% and 16.7%, while for Case 2, the values were 11.5% and 41.7%, both of which were considerably higher than those for Case 1 (Table 2.5). For the SC, the discrepancy in the simulated t_p between Cases 1 and 2 was less significant; however, Case 1 again performed slightly better than Case 2 for more extreme values of θ_i. In particular for Exp. SC5, the relative errors of the simulated t_p were 0% and 33.3% for Cases 1 and 2, respectively (Table 2.5). For Exp. SC1, however, Case 2 actually preformed slightly better with a relative error of 7.1% compared with 14.3% for Case 1 (Table 2.5). For the LS, the results of the simulated t_p for Cases 1 and 2 were rather inconclusive, as neither case preformed particularly well, especially for Exp. LS5 with the highest θ_i (Table 2.5). The better prediction of t_p across more extreme ranges of θ_i for Case 1 for the SCL

and SC may be primarily attributed to the use of θ_e values, which reflect changes in θ_i, unlike the θ_e values for Case 2.

For the LS, both Cases were unable to efficiently predict ponding time across the entire range of θ_i. Errors in simulated from observed t_p for all modeling cases may be attributed to a number of potential reasons including the determination of observed t_p, GA parameter selection, changing surface conditions due to simulated rainfall, and experimental variability. The main focus of this paper, however, is not on ponding time, but rather on GA wetting front prediction.

2.5 CONCLUSIONS

Laboratory infiltration experiments were conducted for three soil types and five initial moisture contents θ_i for each soil. Based on the observed wetting front movement data, a simple mass-balance relationship was developed to determine the GA parameter θ_e, which described the simplified, average effective moisture content of the wetted soil profile. This relationship was effectively used for improved parameterization of a modified GA model in the Hydrol-Inf software by accounting for the underlying model assumptions. An interesting relationship between θ_e and θ_i was identified. It was found that θ_e decreased with increasing θ_i for all three soils, with this relationship more strongly correlated for finer textured soils.

A percent saturation value was also calculated for each θ_e with values much higher for the two finer textured soils (silty clay loam and silty clay) and very low (≈65%) for the coarsest texture soil (loamy sand). The relationships found for the three soil types clearly show the significant effects of both soil texture and θ_i on water movement through soils and strongly support the need for methods for improved estimation of parameters for

changing soil conditions in the GA model. Although the evaluation of the above relationships was only conducted for one rainfall intensity r for each soil type, further investigation into the relationships of θ_e with r and experiments for additional ranges of θ_i may be of interest for future studies.

The improved parameterization method for determining θ_e was applied in the modified GA model in Hydrol-Inf and the observed and simulated wetting front advancement and ponding times were compared. The use of the fitted θ_e values from the above relationships produced more accurate simulation of wetting front movement by Hydrol-Inf across the entire range of θ_i values for all the soil types (Case 1). One additional simplified modeling case (Case 2) was also investigated, in which one constant θ_e was utilized for each soil type across all θ_i values. The Case 2 model produced fairly good agreement between the modeled and observed wetting front depths for the SC and SCL, but did not perform as accurately as the Case 1 model at predicting wetting front movement across the full range of θ_i, particularly the most extreme θ_i values. The Case 2 model, however, proved inefficient at predicting wetting front movement for the loamy sand soil, and significantly under-predicted wetting front movement for all θ_i values. The Case 1 model also provided better simulations of wetting front movement for most experiments associated with different soil types and various initial soil moisture conditions. Further investigations may include the evaluation of this mass balance method for θ_e determination for utilization in the GA model towards expanded wetting front prediction situations and applications including deeper wetting front movement for longer duration experiments.

CHAPTER 3. A NEW METHOD FOR REPLICATING COMPLEX MICROTOPOGRAPHIC SURFACES IN LABORATORY SCALE SOIL BOX EXPERIMENTS[1]

3.1 ABSTRACT

Current laboratory methods for creating rough soil surfaces for surface runoff, infiltration, and soil erosion experiments are limited in their ability to duplicate rough surfaces with uniform soil properties (e.g., bulk density) throughout the soil profile. A new method for replicating rough soil surfaces with uniform bulk density was developed. The new method utilizes a laboratory scale soil box and surface mold constructed with desired rough surface microtopography. For experiments, the surface mold was set on a plane parallel with the bottom of the soil box at a height governed by the desired soil profile depth. The soil box was then rotated 90°; soil was incrementally packed in 5 cm layers in the void volume between the mold and the soil box; the soil box was then rotated 90° back to horizontal; and the surface mold was removed. The ability to replicate rough surface microtopography was verified by creating five rough soil surfaces using the aforementioned method, scanning the surfaces using an instantaneous-profile laser scanner to obtain high resolution DEMs, and determining their maximum ponding area (MPA) and maximum depression storage (MDS) using a Puddle Delineation (PD) program. Each surface was then evaluated by comparing the computed MDS and MPA against the actual

[1] The information in Chapter 3 of this thesis was based on information found in the journal article: "Technical Note: A New Method for Replicating Complex Microtopograpical Surfaces in Laboratory Scale Soil Box Experiments," which was published in 2011 in *Applied Engineering in Agriculture*, volume 27, issue 4, pages 615-620, and was included in this thesis with their written permission. For this technical article, the author of this thesis served as both the primary lead author and researcher of the new method described.

surface mold values. The average MPA and MDS relative errors of the five surfaces from the mold surface were 1.85% and 1.86%, respectively. A separate rough surface also was packed for evaluating bulk density of the packed soil using the replication method. Based on the two-tailed t-test, bulk density was statistically uniform for twelve sample locations across the soil surface and throughout the soil profile. The new method proved efficient and effective at producing soil surfaces with identical rough surface microtopography and uniform bulk density.

3.2 INTRODUCTION AND LITERATURE REVIEW

Various experimental studies on runoff and infiltration have been conducted by packing soil into boxes or flumes and applying artificial rainfall across the surface in a laboratory environment. One limitation of previous studies has been the inability to replicate soil surfaces in subsequent experiments, particularly rough surfaces (Helming et al. 1998; Darboux et al. 2001; Gomez and Nearing 2005) while still achieving uniform soil properties (e.g., bulk density) throughout the soil profile. In practice, a rough surface is often replicated by using similar clod size fractions, which may achieve the same statistical properties associated with random roughness. However, reproducing "photographically" identical surfaces characterized by larger-scale depressions and oriented roughness (systematic elevation variations) has not been realistically feasible. The ability to reproduce photographically identical soil surfaces is particularly important when looking into the dynamics of overland flow generation and connectivity on rough soil surfaces (Darboux et al. 2001), an increasingly relevant topic important to a broad spectrum of fields.

Surface depression storage and its relationship with overland flow generation (or triggering) and depression connectivity are viewed by researchers as a progressively more

valuable relationship in the water resources field, which has received interest in recent years (Darboux et al. 2001, 2002a,b; Martin et al. 2008). Darboux et al. (2001) found that small modifications in surface roughness had a significant effect on overland flow triggering.

Overland flow triggering involves the filling, overflowing, and connection of individual depressions towards an outlet (Darboux et al. 2001) and can significantly affect overland flow. Though the importance in the hydrologic field is well understood, the methods used to quantify runoff triggering are not well agreed upon. Originally, it was perceived that overland flow would commence following the filling of all surface depressions (Mitchell and Jones 1976). Initial attempts to better understand runoff triggering include the use of a cut-and-fill method by Mitchell and Jones (1976) to investigate the effect of micro-relief on the depth of water at which runoff would commence for which. They concluded that total runoff from rough surfaces increases gradually over time. More recent research, however, suggests that runoff from rough surfaces increases intermittently in steps (Hansen 2000) due to the incremental contribution of different depressions as they fill, reach their thresholds, and begin contributing to overland flow.

Better quantification of overland flow initiation is as equally important as quantifying the total runoff volume (Martin et al. 2008). Darboux et al. (2001) concluded that the only effective way to study overland flow genesis was to compare surfaces with identical surface microtopography and depression storage capacities. Additionally, without the ability to achieve uniform bulk densities, the replication of soil surfaces lacks practicality. The achievement of both of these objectives (i.e., replication of soil surfaces

and bulk densities) becomes a feat especially challenging for laboratory experiments. Consequentially, the objective of this study was to develop a new method for replicating complex microtopographic surfaces with uniform bulk density throughout the soil profile when packing soil into soil boxes for laboratory scale experiments. This was accomplished by utilizing a rough surface mold constructed with desired surface microtopography and using calculated maximum depression storage (MDS) and maximum ponding area (MPA) values from the replicated soil surfaces as a method for evaluating surface repeatability. MDS is the total volume of water stored on the surface when all depressions are fully filled and MPA is the total ponded surface area when all depressions are fully filled.

3.3 METHODOLOGY

3.3.1 Soil Box

The 1.0 by 1.2 m soil box consisted of an angle iron frame, a solid steel base with a system for collecting percolating water, four legs mounted on individual casters, and removable clear plexiglass sides bolted to the frame (Fig. 3.1). The two back casters (Fig. 3.1a) were heavy duty (10.2 cm rigid 454 kg Capacity Steel Caster #189244) with slotted wheels, enabling them to be pinned for rotating the soil box. Two, 19-mm holes were drilled in the two front legs of the soil box, through which 19-mm bolts were placed. Two, 20-mm U-Joints, which served as lifting points for rotating the soil box, were slid onto each bolt and held in place with two washers and nuts (Fig. 3.1).

To facilitate side-by-side comparison of different experiments, the soil box was divided by a plexiglass divider positioned down the center (Fig. 3.1b) effectively separating the box into two separate 0.6 m x 1.0 m compartments, thus, actually making it a double soil box. An outlet system capable of simultaneously collecting runoff from the two

separate surfaces was built. The outlet system (Fig. 3.1) was removable for soil packing and was constructed using 18.00 x 2.54 cm lumber and bolted to the soil box.

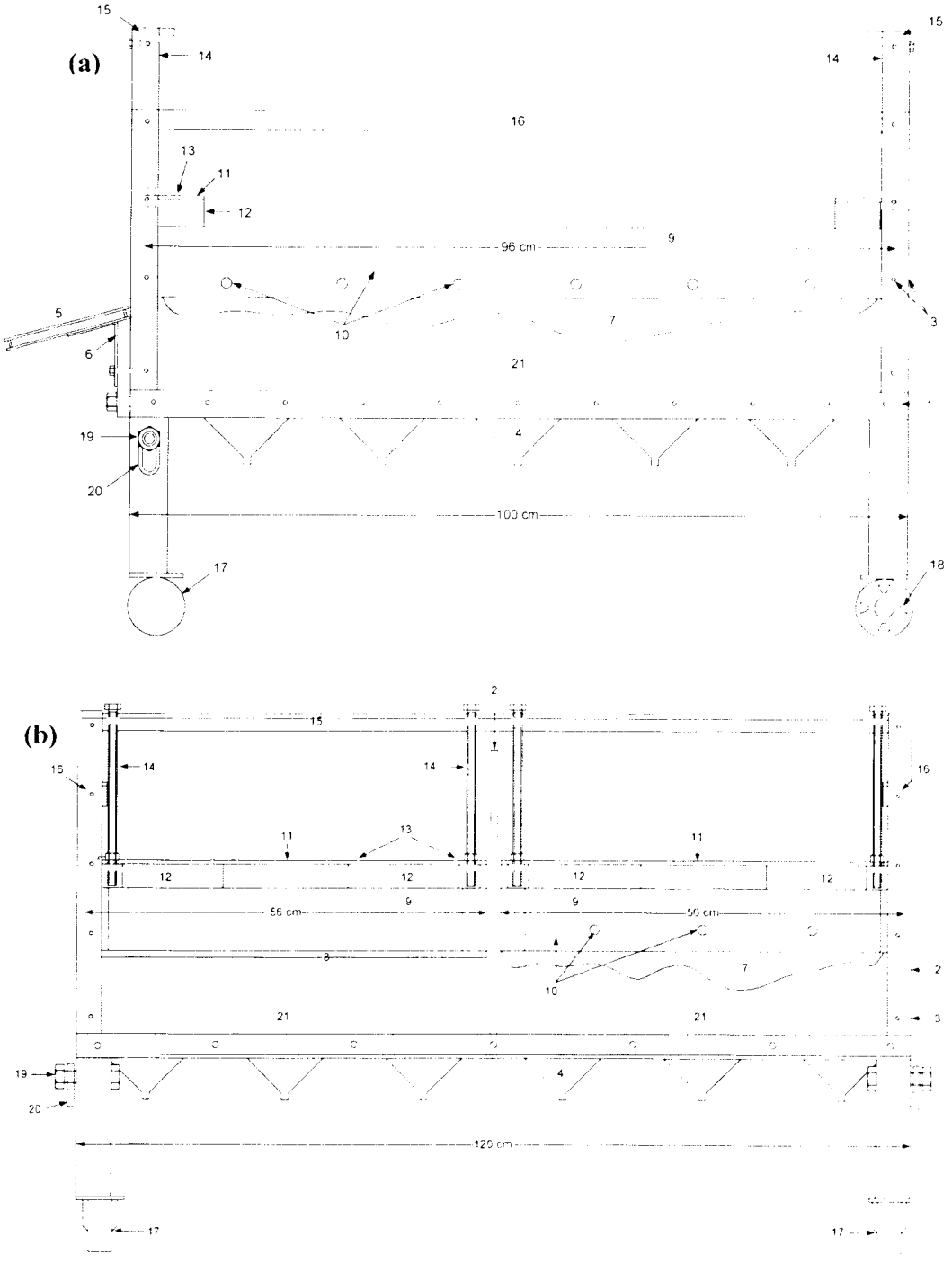

Figure 3.1. Soil box with attached surface molds. (a) Cross-sectional view. (b) Front view. Figures labels described: 1) 38.1 x 38.1 x 4.8 mm angle iron frame; 2) 5.6 mm plexiglass

Figure 3.1. (continued)
sides; 3) 9.52 mm bolts with nuts; 4) Percolation water funnels; 5) Removable outlet; 6) Aluminum brackets; 7) Rough surface; 8) Smooth surface (1.27 cm plywood); 9) Mold Frames; 10) Rebar; 11) 3.81 x 0.32 cm steel anchor plates; 12) 3.81 x 10.16 cm lumber blocking; 13) 4.0 x 0.4 cm leg bolts; 14) 1.27 x 30.48 cm coarse threaded rods (with four nuts/washers each); 15) 51.0 x 51.0x 4.8 mm angle iron (for attaching molds); 16) 38.1 x 38.1 x 4.8 mm angle iron bracing; 17) Light duty casters; 18) Heavy duty casters; 19) 19 mm lifting bolts (with nuts/washers); 20) 20 mm lifting U-Joints; 21) Packed soil profiles.

Five aluminum brackets (4.0 cm wide, 0.3 cm thick, and bent at 75°) were attached to a board and supported the plexiglass construction outlet flow collection system. For each experiment, both 0.6 x 1.0 cm halves of the soil box were packed with soil so that both rough and adjacent smooth soil surfaces were obtained. Further discussions, however, will address only the rough surface compartment as described above, though the smooth surface compartment is visible in Fig. 3.1b.

3.3.2 Surface Mold

To create the mold surface, a rough soil surface was first created in one half of the soil box (0.6 x 1.0 m). The soil surface was designed for overland flow experimental studies and was characterized with a number of depressions of different sizes. The surface included several mini-watersheds with different connectivity configurations of depressions. Around the perimeter of the soil surface, a 3-cm smooth soil "buffer" served as a surface for the wooden mold frame to rest on.

The surface mold was contained within a rectangular wooden frame with outside dimensions of 96 x 56 cm and constructed using 3.81 x 10.16 cm treated lumber. Confined within the frame was #16 rebar, which served to structurally support the concrete surface. The rebar was set in two directions, parallel to both frame sides at 15-cm spacing. To enclose the rebar, 14 mm diameter holes aligned on opposite sides were drilled through the wooden frame 2 cm above the bottom edge on the 96 cm sides and 4 cm above the bottom

on the 56 cm sides. Next, rebar cut to 56 and 96 cm lengths was placed through the coinciding holes on opposite sides of the frame along both sides until aligned flush with the outside edge of the frame on both sides (Fig. 3.1).

The rough soil surface was then covered with 0.05 mm plastic and the wooden mold frame was placed on the covered soil surface (resting on the perimeter "buffer"). Next, Quikrete® Mortar Mix (or other lightweight mold materials) was poured within the frame and allowed to form to the contours of the soil surface. The concrete depth was variable but was leveled to a uniform thickness of 5 cm above the bottom of the wooden frame across the surface to completely cover all rebar. The concrete mold was then covered with 0.05 mm plastic and allowed to cure for three days, after which it was carefully removed from the soil surface.

3.3.3 Attaching the Surface Mold to the Soil Box

Before the soil box could be rotated and packed with soil, the rough surface mold was attached and set on a desired plane parallel to the bottom of the soil box (Fig. 3.1). This plane was governed by the outlet height so that the final packed soil surface, after removal of the surface mold, coincided with the outlet elevation. For setting the surface mold at the desired plane, four 1.27 x 30.48 cm coarse threaded rods with four nuts and washers per rod were attached to each of the four corners of the mold as well as to the soil box frame, thereby allowing for each corner of the mold to be individually raised/lowered to the desired elevation. The threaded rods were attached to the soil box frame using angle iron members (119 cm in length) bolted to the soil box frame and to the surface mold using steel plates bolted to wooden blocking, which was attached to the mold frame (Fig. 3.1).

3.3.4 Frame and Tilting Design

A steel frame and hoist system was constructed for rotating the soil box (Fig. 3.2). The steel frame (2.44 m tall and 1.86 m wide) was constructed using an I-Beam supported vertically on both ends by steel pipe and mounted on 1.84-m rectangular steel tubes. A rail system was built for positioning the soil box underneath the frame using two 1.83-m c-channel members positioned 1.2 m apart, with lumber used to support and brace the rails.

As shown in Fig. 3.2, rotation of the soil box was conducted by first positioning the soil box (with attached surface mold) directly beneath the I-Beam on the rail system. The two back casters of the soil box were then pinned to the rail system using bolts. Next, two hoists (907 kg capacity) attached to the I-beam were hooked to the two lifting U-Joints on the soil box frame (Fig. 3.1). The two hoists were then simultaneously raised until the soil box was resting at 90° on its back (Fig. 3.2b). The soil box was then packed with soil and the procedure reversed.

3.3.5 Soil Packing

After tilting the soil box to 90°, soil was packed in the void space between the mold and the bottom of the soil box in 5 cm layers. The 5 cm layers were chosen based on feasibility of hand packing the entire soil box and achieving uniform layer thickness across the width of the packed layer. For achieving a uniform and known bulk density, a predetermined mass of soil for each layer was calculated based on the void volume, the target bulk density, and the soil moisture content. The mold surface microtopography was incorporated into each layer volume for increased precision by accounting for incremental mold surface feature volumes pertaining to each layer (i.e., subtracting incremental mold feature volumes from total layer volumes).

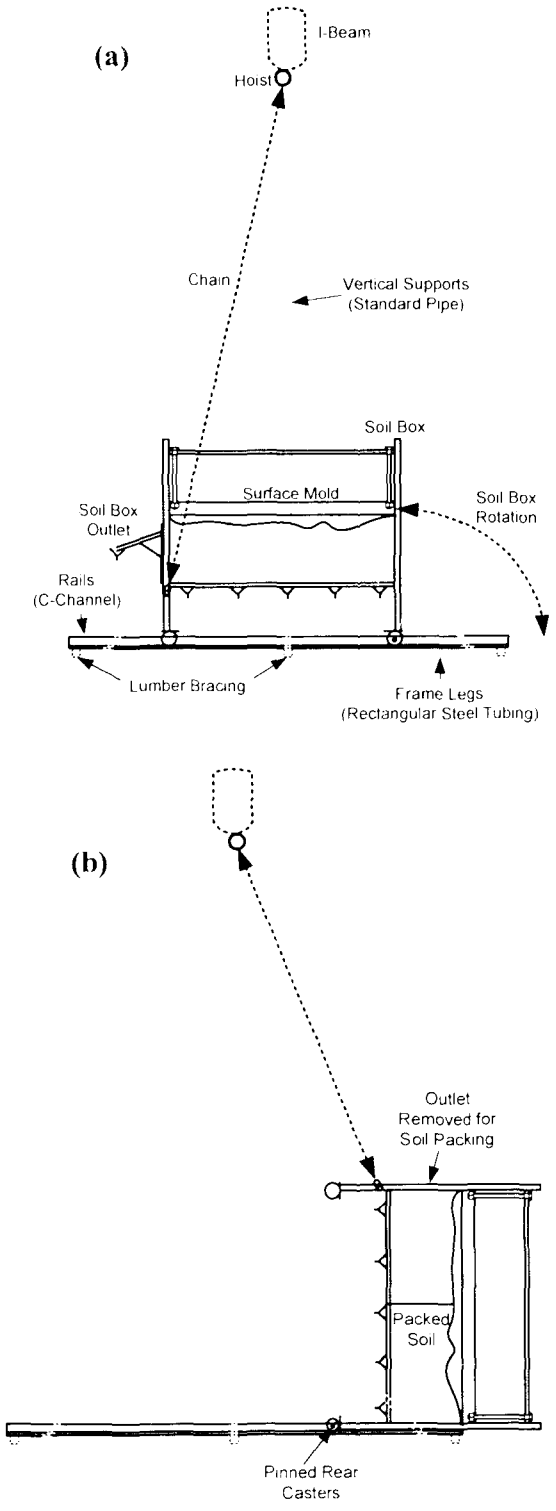

Figure 3.2. Soil box tilting schematic. (a) Soil box at horizontal position. (b) Soil box at 90° tilted position.

A wooden tamp was used for packing soil to predetermined heights in the soil box. Door foam seal tape (2.0 cm wide and 0.7 cm thick) was attached around the bottom perimeter of the mold frame to form a tight seal against the plexiglass sides to prevent soil leakage during packing, with 1 cm round foam door weather strip also used along the 96 cm side of the surface mold to prevent soil loss.

After fully packing the soil box, the soil surface was carefully leveled flush with the soil box frame and the outlet was reattached ensuring that no void spaces were present. Next, using the tilting method, the entire soil box was lowered back down to horizontal and the mold was carefully removed from the soil surface.

3.3.6 Instantaneous-Profile Laser Scanner

To characterize the surface microtopography created using the aforementioned method, an instantaneous-profile laser scanner (Huang and Bradford 1990; Darboux and Huang 2003) was used to obtain microtopographic data. The laser scanner is primarily composed of a camera, two laser diodes, a control box, and a computer. The camera and twin lasers are mounted on a computer-controlled, motorized rail system attached to a 4-m long frame enabling the system to travel lengthwise down the entire frame. The 8-bit monochrome CCD camera in conjunction with the twin laser diodes use triangulation to collect point data from the scanned surface at a rate of one picture per 0.16 s down the length of the frame.

The collected point data are then converted to high resolution DEM data using calibration data based on the laser-camera angle configuration. The laser scanner has resolutions of 0.98 mm horizontally and 0.5 mm vertically. Surfer 8 (Golden Software, Inc., Golden, CO) software was used for the viewing, interpolation, and re-sampling of laser

scanner generated DEM data. It was also utilized to "trim" the additional DEM data obtained by the laser scanner which was outside the range of the soil surface, to construct the input file utilized by the PD program (discussed in the following section) for puddle delineation, and to construct three-dimensional images of soil surfaces.

3.3.7 Surface Characterization and the Puddle Delineation (PD) Program

Various methods have been developed to delineate soil surfaces, characterize surface microtopography, and estimate surface depression storage using DEM data (e.g., Huang and Bradford 1990; Kamphorst et al. 2000; Kamphorst and Duval 2001; Kamphorst et al. 2005). In this study, a recently developed PD program (Chu et al. 2010) was used to characterize surface microtopography and compute MDS and MPA utilizing DEM data. The PD program computes flow directions and accumulations based on the D-8 method (O'Callaghan and Mark 1984). In particular, the PD program is capable of identifying puddles (depressions), their sizes, their overflow thresholds, their contributing cells, and their relationships with adjacent puddles. For instance, one puddle may overflow and discharge to a downstream puddle. If two puddles share a common overflow threshold, they can be combined, forming a higher-level puddle (Chu et al. 2010). Based on the delineation results, the PD program also calculates the MDS and MPA of the surface.

To verify the accuracy of the new method for replicating soil surfaces, the PD program was used to delineate the soil surfaces created using the aforementioned method and determine their MDS and MPA values. Additionally, the rough surface mold was scanned and its DEM was obtained. Since the scanned mold surface was a negative of the actual soil surface, an inverse surface of the scanned rough surface mold and the corresponding DEM were generated. The inverted DEM was then processed using Surfer 8

and subsequent data was input into the PD program for surface delineation and computation of MDS and MPA. Comparison of MDS and MPA of the mold-replicated surfaces and the actual rough surface mold was conducted and evaluated by determining the relative errors and standard deviations.

3.3.8 Surface Replication Procedure

Using the surface replication method, five soil surfaces were created using different soils of varying moisture conditions. The two soils utilized in replications included the Lohnes loamy sand (LS) and Bearden silty clay loam (SCL) introduced in Chapter 2 with specific soil properties also found in Chapter 2. The soil surfaces included four replications using the LS with moisture contents ranging from 0.07 to 0.14 cm^3/cm^3, and one soil surface using the SCL with a moisture content of 0.18 cm^3/cm^3. All soils were air dried and sieved through a 2 mm screen, and additional moisture was then added to achieve the predetermined target moisture contents chosen for each experiment. All packed surface replication profiles were subsequently utilized in overland flow generation experiments for which rainfall was simulated across all surfaces.

After packing the soil box, all soil surfaces were adjusted to a 7% slope. To create the surface slope of the packed soil box, the end opposite from the outlet was raised and set at the desired height using two hydraulic jacks positioned at the two corners of the soil box frame. The surfaces were then scanned and high resolution DEM data were generated (Fig. 3.3).

Additionally, a rough surface was created using the silty clay loam soil with a moisture content of 0.25 cm^3/cm^3 and evaluated solely to determine the effectiveness of the new method at achieving uniform bulk density across the packed soil profiles. Based on the

mass of dry soil and the calculated volume of void space between the surface mold and the bottom of the soil box, the estimated soil bulk density was 946 kg/m^3.

Figure 3.3. Rough surface microtopography and bulk density core sample locations.

Core samples were taken across the soil surface pertaining to various microtopographic features including both peaks and depressions (Fig. 3.3), with the locations and depths of bulk density samples chosen to best represent spatial variations across the soil surface and throughout the profile. Soil sampling depths were 0 - 5 cm and 5 - 10 cm with six samples taken at each depth. Three samples were taken pertaining to both peaks and depressions for each of the two depths along the full length of the soil profile to represent any possible variability. The cylinder used for taking core samples had an i.d. of 50.9 mm and a length of 50.0 mm. All core samples were oven dried at 105°C for 24 h.

Statistical analysis was performed to determine whether a significant difference in the average bulk densities existed between two sampling depths (shallow and deep locations), two main surface topographic features (peaks and depressions), and proximity on the surface to the outlet as attributed to the soil packing method (adjacent to and furthest away from the outlet). Specifically, a two-tailed t-test (McClave and Sincich 2009) was

performed with a criterion of α equal to 0.05 (i.e., 5% probability) for three cases: (1) Case 1: pertaining to depth in the profile, corresponding bulk densities of the six deep and shallow locations were compared using a null hypothesis (H_o) of H_o: μ_{deep} $\mu_{shallow}$; (2) Case 2: for relation to soil surface features, bulk densities located in proximity to the six peak and depression locations were compared using H_o: μ_{peak} $\mu_{depression}$; and (3) Case 3: for proximity to the outlet, the bulk densities of the six locations closest to and furthest from the outlet were compared using H_o: $\mu_{closest}$ $\mu_{furthest}$.

3.4 RESULTS AND DISCUSSION

3.4.1 MDS and MPA

MDS and MPA values of the five surfaces, and their relative errors and standard deviations are summarized in Table 3.1. MDS values ranged from 740 to 799 cm^3 with a standard deviation of 22.7 cm^3 while MPA values ranged from 932 to 972 cm^2 with a standard deviation of 17.3 cm^2, compared to the MDS and MPA of the mold surface of 755 cm^3 and 936 cm^2, respectively. The average relative error of MDS for the five surfaces from the mold surface was 1.85% and the average relative error of MPA from the mold surface was 1.86%. Surface 2 had relative error values of 5.83% for MDS and 3.85% for MPA, which were higher than those of the four other surfaces. One probable reason for the higher relative errors of MDS and MPA of Surface 2 is that the actual slope might have deviated slightly from the target 7% slope. Another possible source of error could have been presented when trimming the edges of the raw surface DEM obtained by the laser scanner even though special care was taken to ensure that the same boundaries were used for all surfaces.

Table 3.1. Maximum Depression Storage (MDS), Maximum Ponding Area (MPA), Standard Deviations, and Relative Errors of the Five Soil Surfaces

Value	Soil Surfaces					Standard Deviation	Surface Mold
	1	2	3	4	5		
MPA (cm^2)	958	972	960	935	932	17.3	936
MPA Relative Error (%)	2.35	3.85	2.56	0.11	0.43	1.57	0
MDS (cm^3)	750	799	760	754	740	22.7	755
MDS Relative Error (%)	0.66	5.83	0.66	0.13	1.99	2.33	0

3.4.2 Bulk Density

For the separate surface created for evaluating the spatial variations of bulk density, the average bulk density and standard deviation across all 12 sample locations (Fig. 3.3) were 903 kg/m^3 and 15.3 kg/m^3, respectively. The bulk densities at the six shallow locations (0 - 5 cm) ranged from 885 to 932 kg/m^3 with an average of 906.2 kg/m^3 and standard deviation of 16.4 kg/m^3. The bulk densities of the six deep locations (5 - 10 cm) ranged from 878 to 915 kg/m^3 with an average and standard deviation of 901 kg/m^3 and 14.8 kg/m^3, respectively.

For Case 1, the resulting p-value of 0.558 was much greater than α and thereby showed no evidence towards rejecting H_0 and indicated no statistical relationship between bulk densities and depth in the soil profile. Similarly, for Case 2, the resulting p-value of 0.711 showed no evidence towards rejecting H_0 and indicated no statistical relationship between bulk densities pertaining to peaks and depressions across the soil surface. For Case 3, the resulting p-value of 0.080 was again greater than α and showed no evidence towards rejecting H_0 and indicated no statistical relationship between bulk density and proximity to the outlet. The only spatial trend in bulk density discovered was slightly higher values closer to the outlet, which may be a result of soil packing and reinstallation of the soil box

outlet. However, the trend was statistically insignificant. Due to uniformity of the sampled bulk densities, it was deemed unnecessary to repeat the procedure for additional soil types.

The initial estimated bulk density based on the total mass of soil and volume (946 kg/m^3) was slightly higher than the average measured bulk density (903 kg/m^3) with a relative difference of 4.2%. One probable reason for this discrepancy is that the volume calculations used for determining the necessary amount of soil needed to achieve a certain bulk density may not have been particularly accurate. This could be attributed to small errors in estimation of the mold surface volume and/or placement of the surface mold above the soil box frame. Overall, the deviation of the predetermined bulk density and the average measured bulk density for the soil profile was small, but illustrates the care that needs to be taken to ensure precise estimation of the void volume and soil mass for determining bulk densities in the soil box. In addition, the bulk density obtained in this experimental study was relatively low. The reason for the low bulk density was most likely due to the moisture content of the soil at packing. However, it should be noted that while the bulk density achieved in this study is lower than typically expected in the field due to the moisture content of the soil at packing, the proposed technique will be valid for packing soils to mimic bulk density more realistic for field soils. Also, no additional soil packing limitations exist for the new method.

3.5 CONCLUSIONS

This study demonstrated a surface replication method effective and efficient at replicating complex microtopographic surfaces. MDS and MPA values were determined for the five replicated surfaces and average relative errors from the rough surface mold MDS and MPA were used to describe repeatability with average values of 1.85% and

1.86%, respectively, for the five surfaces. These errors may be attributed to slight deviations in the actual surface slopes from 7%. Care should be taken to ensure precise final slopes of the soil surface when raising the soil box to the appropriate height. Soil type and initial moisture content had no significant influence on the final surface with the exception that if the soil is too dry, packing may be difficult and the resulting surface following removal of the mold may be loose with a loss of topographical definition.

The new surface replication method was also efficient at producing uniform bulk density across the surface and throughout the soil profile. An overall average bulk density of 903 kg/m^3 was obtained with a standard deviation of 15.3 kg/m^3. The two-tailed t-test showed no statistical differences in bulk densities as attributed to both depth in the soil profile and surface microtopography. The average measured bulk density (903 kg/m^3) deviated slightly from the initial estimated bulk density (946 kg/m^3), which may be accounted for by volume estimates. Thus, care should be taken in obtaining accurate bulk density values in laboratory experiments when no bulk density sampling is performed. The most important point for this study is the ability to achieve uniform soil properties across the mold-created soil surface and throughout the soil profile.

The new surface replication method effectively achieved the desired outcomes of providing the capability of replicating complex microtopographic soil surfaces with uniform bulk densities for subsequent experiments in a laboratory scale soil box. The new packing method is especially useful and applicable for laboratory experimental studies on overland flow and soil erosion and allows for comparison of subsequent experiments with identical soil surface microtopography. This should prove valuable for future experimental

work on the subject areas mentioned, providing much better control over the experimental variables of surface topography and soil properties.

CHAPTER 4. LABORATORY EXPERIMENTS ON THE EFFECT OF MICTOPOGRAPHY ON SOIL-WATER MOVEMENT: SPATIAL VARIABILITY IN WETTING FRONT MOVEMENT

4.1 ABSTRACT

The effect of microtopography on infiltration processes is a major topic of interest for a wide range of disciplines. Particularly, experimental studies investigating the relationship between surface microtopography and infiltration are lacking. Laboratory experiments were conducted by packing soil into small and large boxes and simulating rainfall to investigate the effect of microtopography on infiltration and soil-water movement. In small soil box experiments, the observed wetting fronts from manually cut soil profiles were collected and showed considerably deeper wetting front movement (1.25 - 1.75 cm) beneath a smooth surface area than adjacent depressions for 12 - 60 min duration rainfalls. For large soil box experiments, the times for the wetting front to reach moisture sensors installed at 5 and 10 cm depths relative to various surface microtopographic features were determined across both rough and smooth surfaces. Results showed significant effects of surface microtopography on soil-water movement as the wetting front reached sensors at identical depths below the surface at significantly different times corresponding to surface microtopography. Similar to the small soil box study, wetting front movement was most rapid beneath the smooth surface. Across the rough surface, wetting front movement was "quicker" beneath a surface peak than its adjacent depression. This can be attributed to 2D unsaturated flow. In addition, for both studies, the effect of microtopography on soil-water movement remained evident for deeper soil-water

movement and longer experiment durations. This study provides valuable experimentally-based insight into the effect of microtopography on soil-water movement.

4.2 INTRODUCTION AND LITERATURE REVIEW

Infiltration is controlled by a number of factors including soil capillary suction, initial moisture content, hydraulic conductivity, and pore structure. For practical applications, infiltration is generally considered homogeneous across a soil surface. In reality, infiltration rates often vary significantly and dynamically across a soil surface (Tricker 1981; Sullivan et al. 1996). Infiltration characteristics also strongly influence subsequent water percolation through the vadose zone.

The factors that control spatial and temporal variations in infiltration and soil-water percolation can be divided into three categories: site characteristics, soil characteristics, and meteorological characteristics (Haggard et al. 2005). Site characteristics include slope, microtopography, vegetative cover, grazing conditions, and subsurface conditions; soil characteristics include saturated and unsaturated hydraulic conductivity, degree of aggregation, bulk density, and the presence of macropores; and meteorological characteristics include rainfall intensity, duration, and spatial variations (Haggard et al. 2005). Antecedent soil moisture condition is another important site and soil characteristic which exerts a significant influence on soil water movement in soils (Bissonnais et al. 1995; Magunda et al. 1997; Haggard et al. 2005; Wei et al. 2007).

Microtopography is a site characteristic that can affect spatial variations in infiltration and soil-water percolation directly and indirectly, and is a research area in need of significantly more work (Grovers et al. 2002). Generally, increasing soil roughness will result in increased infiltration (Burwell and Larson 1969; Helming et al. 1998; Gomez and

Nearing 2005) and varying microtopography will result in varying infiltration rates (Dunn et al. 1991).

Surface microtopography may affect spatial variations in infiltration through its influence on surface ponding. It is well accepted that a rougher surface has greater depression storage and surface ponding compared to a smooth surface (Mitchell and Jones 1976; Onstad 1984; Darboux et al. 2001). Increased ponding depth will increase infiltration due to the inundation of more surface area and increased ponding head (Dunne et al. 1991; Fox et al. 1997; Fox et al. 1998a, b; Assouline and Ben-Hur 2006).

Microtopography may also influence spatial variations in infiltration as attributed to its role in the development of surface sealing (Magunda et al. 1997; Fox et al. 1998a, b; Assouline 2004). Structural seals form due to aggregate breakdown as a direct result of rainfall impact and generally are most prevalent on surface peaks, while sedimentary seals are associated with the deposition of sediments in surface depressions (Fox et al. 1998b). Structural seals generally have much higher hydraulic conductivities than sedimentary seals (Fox et al. 1998a, b). During a rainfall event, structural seal formation generally occurs earlier while sedimentary seals develop more slowly (Fox et al. 1998b). Seal formation may also be effected by surface ponding due to the protection from raindrop impact the ponded water surface provides to the soil surface.

The significant influence of microtopography on spatial variations in infiltration subsequently translates directly towards its considerable influence on soil-water percolation by its control over the location and amount of water entering the soil. Both matric and gravitational forces control water movement in the soil. 2D trends in soil-water movement beneath a rough surface of peaks and depressions may include significant horizontal

wetting front movement as attributed to strong matric relative to gravitational forces initially acting on water in soil, after which gravitational forces generally become predominant with time (Hillel 1998).

To the best of our knowledge, very limited experimental work has been conducted evaluating infiltration variability and subsurface soil-water movement characteristics as affected by surface microtopography. The objective of this research is to investigate the effect of microtopography on infiltration and soil-water movement by conducting a set of laboratory-scale, small and large soil box experiments under simulated rainfalls across both smooth and rough surfaces. Soil moisture data pertaining to different surface microtopographic features were collected and utilized to examine the spatial variability in both wetting front movement and soil moisture content associated with different surface microtopographic characteristics.

4.3 METHODOLOGY

4.3.1 Soil Box and Soil

A set of laboratory-scale soil box experiments were conducted by packing soil into two different soil boxes (small and large). The 30 x 30 cm small box was built with a wooden frame and clear plexiglass sides, and was designed with the capability of packing soil to a uniform bulk density (ρ_b) while incorporating a surface mold. A small surface mold 30 x 30 cm, which allowed for the replication of soil surfaces, was created with the desired surface microtopography. The mold was attached to the top of the empty soil box using a small removable frame; the soil box was rotated upside down; and soil was packed uniformly in 2.5 cm layers to achieve a predetermined bulk density. A level surface flush with the soil box sides was then created; the bottom of the soil box was re-attached; the soil

box was rotated 180° (back to right side up); and the mold was removed. The resulting soil surface was an exact replication of the surface mold with a uniform ρ_b throughout the soil profile pertaining to smooth areas, depressions, and peaks. One side of the soil box was removable so that the soil profile could be manually cut in order to evaluate the wetting front location within the soil profile corresponding to different surface microtopographic features.

For the large soil box experiments, a 100 x 120 cm soil box was utilized. Sande et al. (2011) detailed the soil box, a mold of desired surface microtopography, and the procedures for soil packing and surface creation, which can also be found in Chapter 2. One of the key features of the method is the capability to replicate rough soil surfaces while maintaining uniform ρ_b throughout the soil profile. Additionally, the soil box incorporates a divider placed down the center of the box creating adjacent 60 x 100 cm smooth and rough soil surfaces for each packed soil box to facilitate simultaneous side-by-side comparison of experiments for two distinct surface microtopographic conditions (Sande et al. 2011).

For both small and large soil box experiments, the Lohnes loamy sand (LS) soil introduced in Chapter 2 was utilized with specific soil properties found in Chapter 2. Four small soil box experiments were conducted with similar initial moisture contents (θ_i) ranging from 0.063 - 0.080 cm^3/cm^3, while two large soil box experiments were conducted using two different θ_i values of 0.073 and 0.144 cm^3/cm^3. The θ_i values were determined experimentally based on the gravimetric moisture content and ρ_b. Basic experimental information and major soil property parameters are shown in Table 4.1.

Table 4.1. Basic Experimental Information and Soil Properties

Exp[a]	Soil[b]	Surface Condition	Surface Size(s) (cm)	θ_i[c] (cm^3 cm^{-3})	ρ_b[d] (kg m^{-3})	r[e] (cm hr)	Surface Slope (%)	Duration (min)
S1	LS	Rough	30 x 30	0.063	1.400	3.80	0	12
S2	LS	Rough	30 x 30	0.059	1.400	3.80	0	20
S3	LS	Rough	30 x 30	0.080	1.400	3.80	0	40
S4	LS	Rough	30 x 30	0.064	1.400	3.80	0	60
L5	LS	Rough and Smooth	60 x 100	0.073	1.400	5.79	7	120
L6	LS	Rough and Smooth	60 x 100	0.144	1.400	5.79	7	78

[a] S is the small soil box (30 x 30 cm) and L is the large soil box (120 x 100 cm)
[b] LS is the loamy sand soil
[c] θ_i is the initial moisture content
[d] ρ_b is the bulk density
[e] r is the rainfall intensity

4.3.2 Surface Topography

For both the small and large soil boxes, surface microtopography was obtained using an instantaneous-profile laser scanner (Huang and Bradford 1990; Darboux and Huang 2003) which is further described in Chapter 3. The small soil box surface consisted of two depressions and an adjacent smooth surface (Fig. 4.1). For the large soil box surface, the aforementioned smooth and rough soil surfaces are shown in Fig. 4.2. More design criteria for the rough soil surface of the large soil box can be found in Sande et al. (2011).

4.3.3 Norton Style Rainfall Simulator

A Norton-style rainfall simulator (Meyer and Harmon 1979; Meyer 1994) utilizing four oscillating VeeJet nozzles was used to simulate rainfall across soil surfaces in this study. The rainfall simulator was introduced in Chapter 2, and additional information on the simulator may be found at that location. The simulator was calibrated for lab-specific conditions for the entire theoretical coverage area beneath the simulator. Placement of the small and large soil boxes was selected based on the calibrated rainfall distributions as the area(s) with the most uniform distribution of rainfall intensities. The average rainfall

intensities for the small and large soil box experiments were 3.80 and 5.79 cm/hr, respectively (Table 4.1).

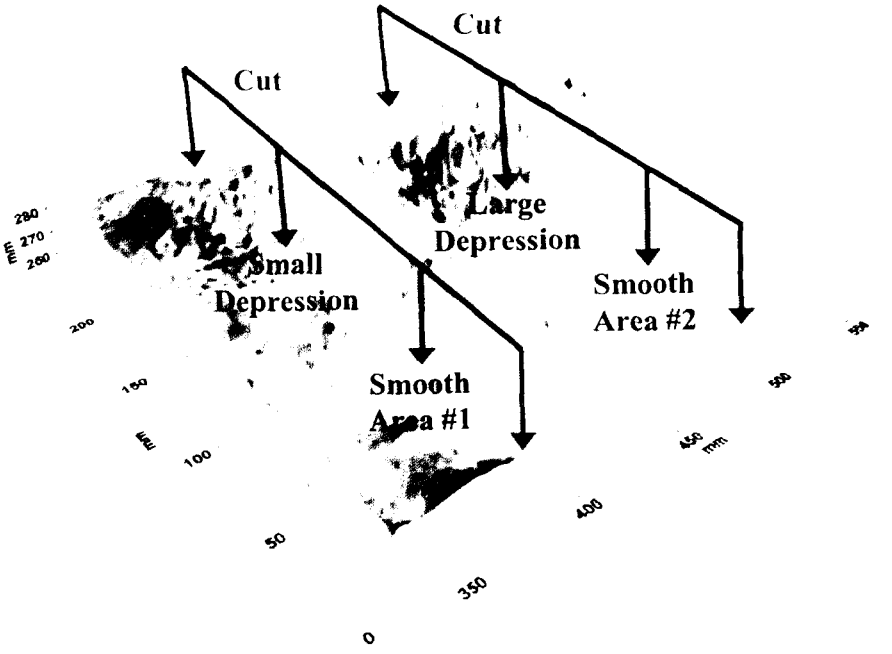

Figure 4.1. Small soil box surface microtopography and soil profile cutting locations.

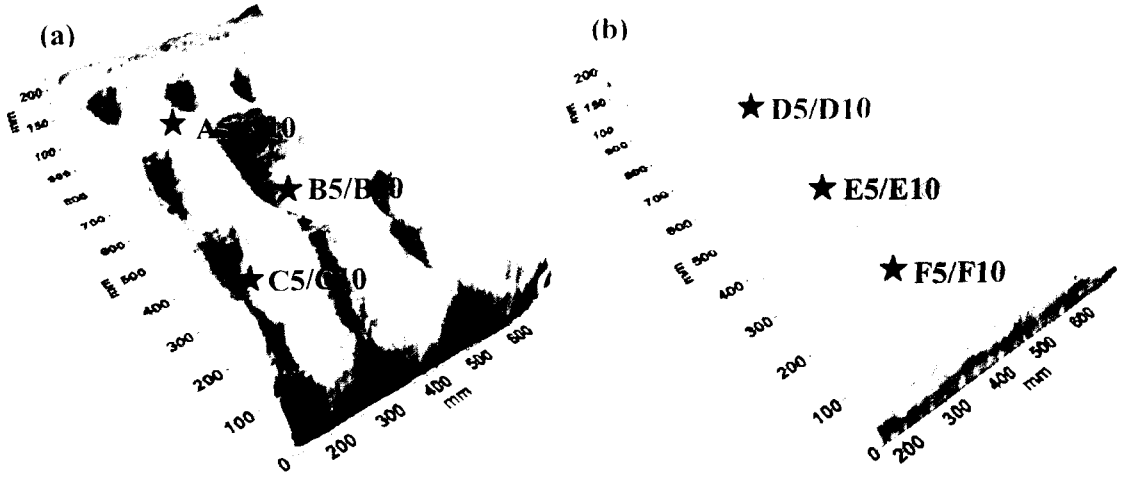

Figure 4.2. Large soil box surface microtopography and moisture sensor locations at depths of 5 and 10 cm for both rough and smooth surfaces. (a) Rough surface. (b) Smooth surface.

4.3.4 Soil Moisture

For the small soil box experiments, the visible wetting front within the soil profile was collecting at the conclusion of rainfall events by cutting the soil profile and measuring the depth from the surface to the observed wetting front. The soil profile was manually cut following the simulated rainfall at two locations (Fig. 4.1). The depth of the observed wetting front relative to the soil surface was obtained pertaining to three surface features shown in Fig. 4.1: the large depression, the small depression, and the smooth areas (including Smooth Area #1 and #2 in Fig. 4.1). Four small soil box experiments with similar θ_i values and different durations were conducted so that wetting front characteristics pertaining to different surface feature could be collected for a range of different rainfall durations (i.e., 12 - 60 min, Table 4.1). For each experiment, only one set of wetting front depths within the soil profile could be collected as attributed to the fact that rainfall was discontinued and the soil profile was cut.

For the large soil box experiments, soil moisture data were collected utilizing moisture sensors installed in soil profiles to investigate the effect of microtopography on soil-water movement. Soil moisture was measured in each experiment at 1-min intervals using Decagon EC-5 (Pullman, Washington) moisture sensors installed parallel to the soil surface at depths of 5 and 10 cm at various locations within the soil profiles beneath both the smooth and rough surfaces (Fig. 4.2). In the Fig. 4.2, sensor notations of 5 and 10 refer to 5 and 10 cm depths. For the rough surface, two moisture sensors (A5 and A10) were placed beneath a surface peak while the remaining four sensors were located beneath two major depressions (Fig. 4.2a).

4.3.5 Evaluating the Effect of Microtopography on Soil-Water Movement

The procedures of both small and large soil box experiments involved packing the boxes with soil, scanning the surface(s) with the laser scanner, positioning the soil box beneath the rainfall simulator, and simulating rainfall across the soil surface(s). For the small soil box experiments, rainfall was simulated across the soil surfaces for predetermined periods of time ranging from 12 to 60 min (Table 4.1). Following rainfall, the side of the soil box was removed and wetting fronts relative to the surface at the two cut locations (Fig. 4.1) were immediately recorded before continued moisture redistribution occurred (within 1 - 2 min). Final wetting front depths across the four experimental durations were then used directly for analysis.

In the large soil box experiments, rainfall was simulated across the soil surfaces until the entire surface areas (both rough and smooth surfaces) were fully ponded and contribute runoff to the outlet. Data, including wetting front, outlet flow, and surface ponding status, were collected during the experiments. For analysis of the laboratory soil moisture sensor data, time for the advancing wetting front to reach each moisture sensor (t_{wcf}) was determined. These times were determined as the ones when the first significant step increase in moisture content (θ) from θ_i was observed. As a verification of this method for determining t_{wcf}, the sensor t_{wcf} values were also compared with the observed wetting front data. It was found that the sensor t_{wcf} consistently represented a time slightly before arrival of the observed wetting front at the depth of the actual moisture sensors. This can be primarily attributed to the zone of influence and sensitivity of the moisture sensor. The concentration for this study, however, is on examining the differences in the t_{wcf} values

between the rough and smooth surfaces. Thus, consistency in the sensor t_{wet} values was most important as opposed to exact t_{wet} and θ values.

4.4 RESULTS AND DISCUSSION

4.4.1 The Effects of Microtopography on Soil-Water Movement Characteristics

4.4.1.1 Small Soil Box Experiments

Final wetting front depths at the three surface locations (i.e., large and small depressions and smooth areas) for the four small soil box experiments are shown in Table 4.2. For all experiments, the final wetting front depths relative to the surface beneath the smooth areas were deeper than those in both the large and small depressions. Compared with the large depression, the final wetting front depths were 1.25 - 1.75 cm deeper beneath the smooth area (Average of Smooth Area #1 and #2 as aforementioned, Fig. 4.1 and Table 4.2), with similar values for the small depression compared with the smooth area (Average of Smooth Area #1 and #2, Fig. 4.1). The final wetting front depths beneath the large and small depressions were similar for short duration experiments (i.e., Exp. S1 and S2, Table 4.2). However, slightly deeper final wetting fronts were observed beneath the smaller depression for longer duration experiments (i.e., Exp. S3 and S4, Table 4.2).

Table 4.2. Small Soil Box Final Cut Wetting Front Depths

	Surface Location		
Exp[a]	Large Depression	Small Depression	Smooth Area
S1 WF (cm)	3.00	3.00	4.50
S2 WF (cm)	5.00	4.75	5.75
S3 WF (cm)	8.50	9.00	9.75
S4 WF (cm)	13.00	13.50	14.75

[a]S1 - S4 refer to Exp. S1 - S4, respectively; and WF is the final cut wetting front depth relative to the surface

Overall results from the small soil box experiments clearly show increased wetting front movement depths relative to the surface associated with the smooth area compared

with microtopographic depressions. In addition, the discrepancy in final wetting front depths between the smooth area and both depressions relative to the surface stayed nearly identical across all four experiment durations of 12 - 60 min. These results show that even for the longest experiment duration utilized (i.e., 60 min), the effect of microtopography on wetting front movement is still very evident.

4.4.1.2 Large Soil Box Experiments

Moisture sensor data for large soil box experiments Exp L5 and L6 (Table 4.1) were collected and are shown in Figs. 4.3 and 4.4. Compared with the smooth surface, high variability in soil-water movement characteristics can be observed for the rough surface for Exp L5 and L6 (Figs. 4.3 and 4.4). Based on the sensor-recorded soil moisture data for shallow and deep depths of both the smooth and rough surfaces (Fig. 4.2), t_{wcf} values were determined for all sensors and are shown in Table 4.3.

Table 4.3. Large Soil Box Wetting Front Times (t_{wcf})

Sensor	Exp. L5[a] t_{wcf}[c] (min)	Exp. L6[b] t_{wcf}[c] (min)
A5	14	11
B5	12	12
C5	18	13
D5	10	9
E5	11	10
F5	11	10
A10	27	27
B10	33	28
C10	43	34
D10	28	27
E10	29	24
F10	27	25

[a] L5 refers to Exp. L5 with θ_i = 0.073 cm^3 cm^{-3}
[b] L6 refers to Exp. L6 with θ_i = 0.144 cm^3 cm^{-3}
[c] t_{wcf} is the time for the wetting front to reach the sensor

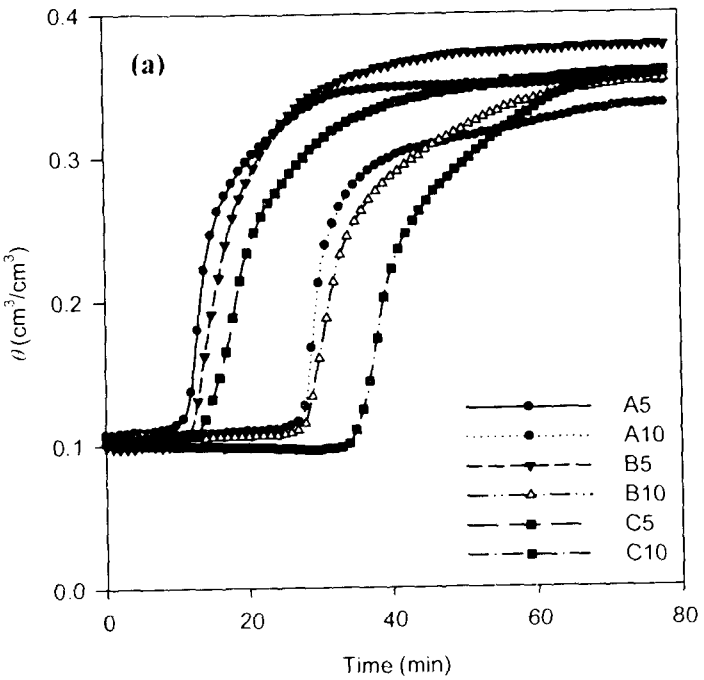

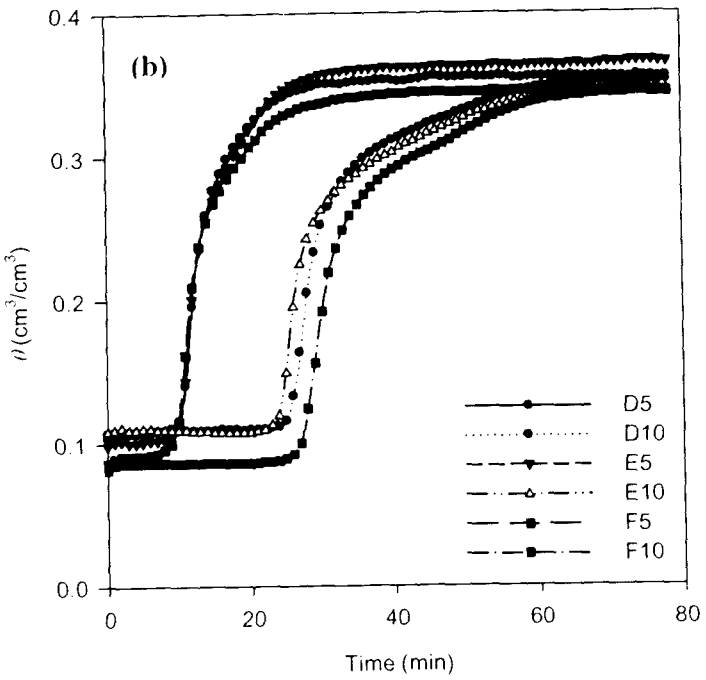

Figure 4.3. Large soil box moisture sensor data for initial water content $\theta_i = 0.144$ cm^3/cm^3 for both the smooth and rough surface. (a) Rough surface. (b) Smooth surface.

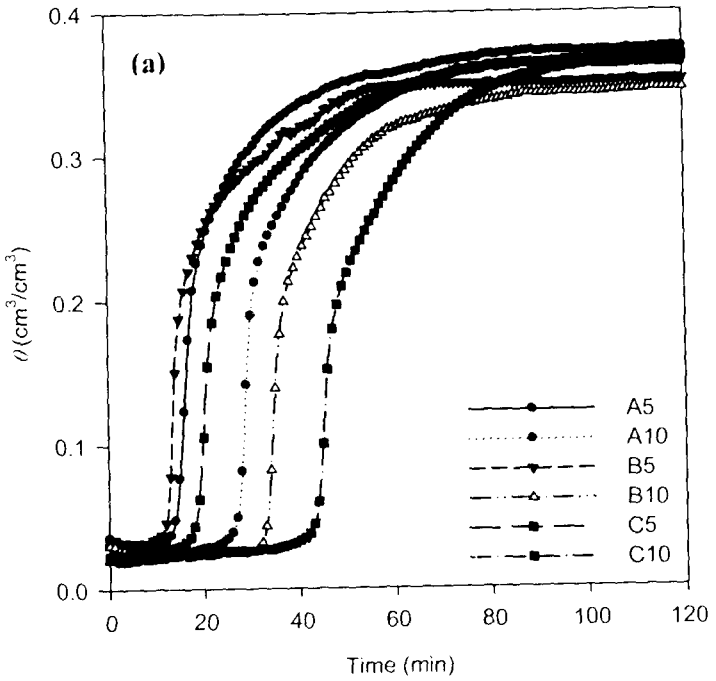

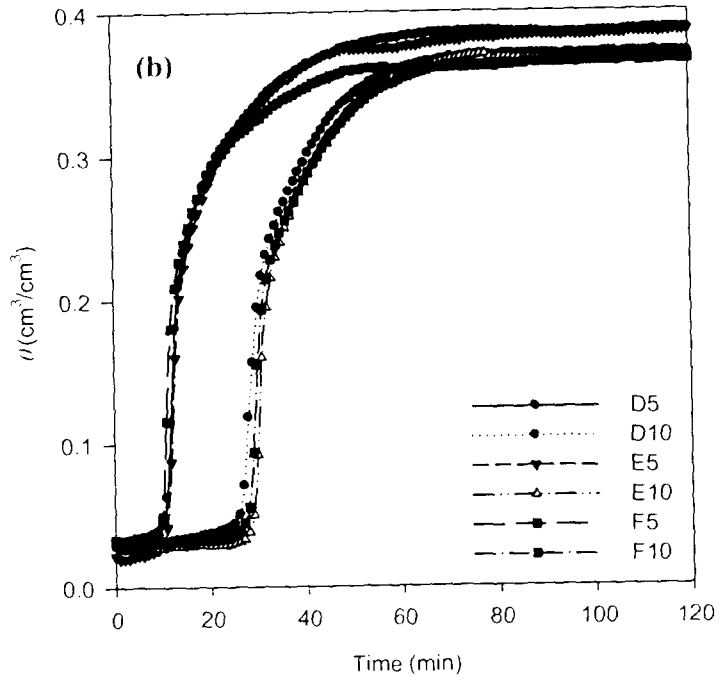

Figure 4.4. Large soil box moisture sensor data for initial water content $\theta_i = 0.073$ cm^3/cm^3 for both the smooth and rough surface. (a) Rough surface. (b) Smooth surface.

The t_{wet} values for the smooth surface were in very close agreement with each other across the three shallow and deep moisture sensors for both Exp L5 and L6 (Table 4.3), which shows the uniformity in soil-water movement beneath the smooth surface. For the rough surface, the variability in t_{wet} values across the sensors were large compared with the smooth surface values. Particularly for the rough surface deep moisture sensors, the range in t_{wet} values between maximum and minimum t_{wet} values across the three deep sensors were 16 and 7 min for Exp L5 and L6, respectively (Table 4.3).

Compared with smooth surface sensor t_{wet} values, all rough surface sensor t_{wet} values pertaining to both peaks and depressions were greater for both Exp L5 and L6. However, sensors A5 and A10 pertaining to the surface peak had t_{wet} values and the subsequent wetting front movement characteristics that were very close to those observed beneath the smooth surface. The rough surface sensors located beneath the surface depressions (particularly sensors C5 and C10), had t_{wet} values (and the subsequent wetting front movement characteristics) which were consistently larger than those observed beneath the smooth surface. This general finding of increased wetting front movement beneath high-elevation peaks was similar to that observed in the small soil box experiments. Also similar to the small soil box experiments, the effect of microtopography on soil-water movement was very evident for longer duration experiments. As the wetting front moved deeper in the soil profile, the discrepancy between deep moisture sensor t_{wet} values pertaining to different surface features increased, that is, there was increasing variability in t_{wet} values across sensors pertaining to different surface microtopographical features as the wetting front moved deeper in the soil profile.

4.4.2 Further Soil-Water Movement Discussions

Several potential effects of microtopography on soil-water movement characteristics may contribute to the findings observed in this study for both the small and large soil box experiments, particularly in wetting front movement characteristics. One effect of microtopography on soil-water movement, which may have contributed to increased wetting front movement relative to the smooth surface (small and large soil box) and the surface peak (large soil box), can be attributed to the matric and gravitational forces acting on soil-water movement. For uniform rainfall on a smooth surface, soil-water movement is primarily along the vertical direction as the wetting front moves downwards with both gravitational and matric (due to the dry soil located directly beneath the advancing wetting front) forces acting in the vertical direction. Beneath a rough surface of peaks and depressions, however, matric relative to gravitational forces may be particularly strong in horizontal directions initially, as attributed to the dry soil located in a radial direction both towards the "center" of peaks and outwards surrounding the boundaries of depressions. These characteristics may lend themselves towards a tendency of "converging" and "diverging" wetting front patterns beneath peaks and depressions, respectively. In addition, for a surface of only depressions and smooth areas (i.e., small soil box surface), the depressions may contribute to increased wetting front movement beneath the adjacent smooth areas as attributed to the aforementioned reasons. Together, these trends and 2D/3D unsaturated flow likely contributed to the increased wetting front movement relative to the surface for the smooth surface for both the small and large soil box experiments as well as the lower $t_{w,f}$ values for the large soil box experiments pertaining to the peak compared with depressions for the rough surfaces.

Another possible effect of microtopography on soil-water movement characteristics in this study may be attributed to its influence on surface ponding and resulting preferential infiltration. As no surface ponding was observed in the small soil box experiments, discussion on this effect will focus on the large soil box experiments. For Exp L5, no surface ponding was observed on either the rough or smooth surface before the wetting front reached any sensors. For Exp L6, however, surface ponding occurred before the wetting front reached the deep sensors for both the smooth and rough surfaces. In particular, for sensors B5 and B10 of the rough surface (Fig. 4.2a), surface ponding at that location was first observed at 17 min, which may have contributed to the shorter t_{wet} values for the deep sensor (B10). Still, t_{wet} values at that location (B10) were high compared with those pertaining to both the peak (A10) and smooth surface (D10, E10 and F10) sensors (Table 4.3), even with the additional effect of surface ponding.

The wetting front movement trends observed in the small and large soil box experiments also may be attributed to the potential effect of microtopography on seal formation. Depressions are generally associated with the formation of lower hydraulic conductivity sedimentary seal formation due to the accumulation of sediments, while peaks and smooth areas are associated with the formation of higher hydraulic conductivity structural seal formation due to raindrop impact. It's possible, for both small and large soil box experiments, that the trend of decreased wetting front movement relative to the surface beneath depressions may be related to seal formation. However, this issue is out of the focus of this experimental study.

of 1D/2D/3D unsaturated flow under influence of surface microtopography against experimental results will definitely improve our understanding of the underlying processes and mechanisms.

CHAPTER 5. OVERALL CONCLUSIONS AND FUTURE WORK

This thesis presents a broad spectrum of experimentally based research on infiltration and soil-water movement. In Chapter 2 small scale infiltration studies were conducted and used to improve wetting front prediction capabilities of a modified Green-Ampt (GA) model across changing initial soil conditions. A practical, mass-balance based effective water content θ_e was proposed for several soil types and different initial water content θ_i values as the average water content θ above the advancing wetting front. The strong influence of θ_i on wetting front movement was observed and an interesting relationship of decreasing θ_e with increasing θ_i was found to exist for three soil types. θ_e values were then incorporated into the GA model in place of θ_s to help account for different soil moisture conditions and wetting front movement characteristics. This work aids in expanding the capabilities of the GA model as well as exposes some key assumptions which must be considered for its effective application.

Future work may further investigate the θ_e - θ_i relationships as well as their applicability in the GA modeling for field situations. The applicability of this relationship under different surface ponding status may also be further investigated in addition to the possible utilization of observed surface ponding status under simulated rainfall towards the calibration of GA effective hydraulic conductivity as was accomplished in Chapter 2.

In Chapter 3, a method which effectively allowed for the replication of complex surface microtopography with uniform bulk densities while packing soil into soil boxes for laboratory scale infiltration/runoff experiments was introduced. The new capabilities presented by the method offer a wide array of possibilities towards experimental studies

evaluating the effect of different surface microtopographical conditions on infiltration, runoff, surface erosion, and tracer transport for different initial soil moisture conditions.

In Chapter 4, laboratory experimental studies were conducted at two scales by subjecting packed soil surfaces to simulated rainfall to evaluate the effect of surface microtopography on infiltration and soil-water movement. For experiments, soil-water movement data pertaining to different surface microtopographic features was collected utilizing moisture sensors installed within soil profiles as well as the visible wetting front as observed within cut soil profiles for different durations of simulated rainfall. The strong influence of surface microtopography was observed in the variability in soil-water movement characteristics between rough surfaces and smooth surface features. Wetting front movement relative to the soil surface was much more rapid pertaining to soil surface smooth areas and peaks compared with adjacent depressions. This may be attributed to the concept of converging and diverging wetting front characteristics pertaining to peaks and depressions as attributed to the matric and gravitational forces influencing soil-water movement.

Based on the experimental work, future experimental studies may be conducted further investigating the effect of microtopography on soil-water movement characteristics. In particular, further experimental studies utilizing additional surface conditions, soil conditions, scales, and rainfall events may be valuable. Field scale experimental studies under natural field conditions may also prove valuable.

Based on the experimental work, one of the major future objectives is towards improved modeling capabilities and prediction of field infiltration and soil-water movement processes. Still, before an expansion of modeling capabilities, an improved

understanding of actual processes based on experimental work and observations is imperative.

LITERATURE CITED

Assouline, S. (2004). "Rainfall-induced soil surface sealing: a critical review of observations, conceptual models, and solutions." *Vadose Zone J.*, 3(2), 570-591.

Assouline, S., and Ben-Hur, M. (2006). "Effects of rainfall intensity and slope gradient on the dynamics of interrill erosion during soil surface sealing." *Catena*, 66(3), 211-220.

Beven, K. (1984). "Infiltration into a class of vertically non-uniform soils." *Hydrolog. Sci. J.*, 29(4), 425-434.

Bissonnais, Y. L., Renaux, B., and Delouche, H. (1995). "Interactions between soil properties and properties and moisture content in crust formation, runoff and interrill erosion from tilled loess soils." *Catena*, 25(1-4), 33-46.

Bodman, G. B., and Colman, E. A. (1944). "Moisture and energy conditions under downward entry of water into soils." *Soil Sci. Soc. Am. J.*, 8, 116-122.

Bouwer, H. (1966). "Rapid field measurement of air-entry value and hydraulic conductivity of soil as significant parameters in flow system analysis." *Water Resour. Res.*, 2(4), 729-738.

Bouwer, H. (1969). "Infiltration of water into nonuniform soil." *J. Irrig. Drain. E.*, ASCE, 95(IR4), 451-462.

Brakensiek, D. L. (1977). "Estimating the effective capillary pressure in the Green and Ampt infiltration equation." *Water Resour. Res.*, 13(3), 680-682.

Brooks, R. H., and Corey, A. T. (1964). *Hydraulic properties of porous media. Hydrology Paper No. 3*, Colorado State University, Fort Collins, Colorado.

Burdine, N. T. (1953). "Relative permeability calculations from pore size distribution data." *Petroleum Translations*, American Institute of Mining Engineering, 198, 755-769.

Burwell, R. E., and Larson, W. E. (1969). "Infiltration as influenced by tillage-induced random roughness and pore space." *Soil Sci. Soc. Am. Pro.*, 33, 449-452.

Childs, E. C., and Bybordi, M. (1969). "The vertical movement of water in stratifies porous material 1. Infiltration." *Water Resour. Res.*, 5(2), 446-459.

Chu, S. (1978). "Infiltration during an unsteady rain." *Water Resour. Res.*, 14(3), 461-466.

Chu, X., and Mariño, M. A. (2005). "Determination of ponding condition and infiltration into layered soils under unsteady rainfall." *J. Hydrol.*, 313(3-4), 195-207.

Chu, X., and Mariño, M. A. (2006). "Simulation of infiltration and surface runoff A Windows-based hydrologic modeling system HYDROL-INF." Examining the Confluence of Environmental and Water Concerns, *Proc., 2006 World Environmental and Water Resources Congress*, edited by R. Graham, ASCE, 1-8.

Chu, X., Zhang, J., Chi, Y., and Yang, J. (2010). "An improved method for watershed delineation and computation of surface depression storage." Watershed Management 2010: Innovations in Watershed Management Under Land Use and Climate Change, *Proc., 2010 Watershed Management Conference*, edited by K. W. Potter and D. K. Frevert, ASCE, 1113-1122.

Darboux, F., Davy, P., Gascuel-Odoux, C., and Huang, C. (2001). "Evolution of soil surface roughness and flowpath connectivity in overland flow experiments." *Catena*, 46(2), 125-139.

Darboux, F., Davy, P., and Gascuel-Odoux, C. (2002a). "Effect of depression storage capacity on overland-flow generation for rough horizontal surfaces: water transfer distance and scaling." *Earth Surface Processes*, 27(2), 177-191.

Darboux, F., Gascuel-Odoux, C., and Davy, P. (2002b). "Effects of surface water storage by soil roughness on overland-flow generation." *Earth Surface Processes*, 27(3), 223-233.

Darboux, F., and Huang, C. (2003). "An instantaneous-profile laser scanner to measure soil surface microtopography." *Soil Sci. Soc. Am. J.*, 67(1), 92-99.

Dunne, T., Weihua, Z., and Aubry, B. F. (1991). "Effects of rainfall, vegetation, and microtopography on infiltration and runoff." *Water Resour. Res.*, 27(9), 2271-2285.

El-Shafei, Y. Z., and Al-Darby, A.M.. (1991). "Initial moisture content in relation to infiltration capacity of sandy soils." *Journal King Saud University. Agricultural Sciences*, 3(2), 333-348.

Faybishenko, B. A. (1995). " Hydraulic behavior of quasi-saturated soils in the presence of entrapped air: Laboratory experiments." *Water Resour. Res.*, 31(10), 2421-2435.

Fayer, M. J., and Hillel, D. (1944). "Air encapsulation: I. measurement in a field scale." *Soil Soil Sci. Soc. Am. J.*, 50, 568-572.

Fox, D., Bryan, R., and Price, A. (1997). "The influence of slope angle on final infiltration rate for interrill conditions." *Geoderma*, 80(1-2), 181-194.

Fox, D., Bissonnais, Y., and Quetin, P. (1998a). "The implications of spatial variability in surface seal hydraulic resistance for infiltration in a mound and depression microtopography." *Catena*, 32(2), 101-114.

Fox, D., Bissonnais, Y., and Bruand, A. (1998b). "The effect of ponding depth on infiltration in a crusted surface." *Catena*, 32(2), 87-100.

Gomez, J. A., and Nearing, M. A. (2005). "Runoff and sediment losses from rough and smooth soil surfaces in a laboratory experiment." *Catena*, 59(3), 253-266.

Green, W.H., and Ampt, G. (1911). "Studies in soil physics, part I – the flow of air and water through soils." *J. Agr. Sci.*, 4, 1-24.

Grovers, G., Takken, I., and Helming, K. (2000). "Soil roughness and overland flow." *Agronomie*, 20(2), 131-146.

Haggard, B. E., Moore Jr., P. A., and Brye, K. R. (2005). "Effect of slope on runoff from a small variable box-plot." *Journal of Environmental Hydrology*, 13(25), 1-8.

Hammecker, C., Antonino, A. C. D., Maeght, J. L., and Boivin, P. (2003). "Experimental and numerical study of water flow in soil under irrigation in northern Senegal: evidence of air entrapment." *Eur. J. Soil Sci.*, 54(3), 491-503.

Hansen, B. (2000). "Estimation of surface runoff and water-covered area during filling of surface microrelief depressions." *Hydrol. Process.*, 14(7), 1235-1243.

Helming, K., Romkens, M. J., and Prasad, S. N. (1998). "Surface roughness related processes of runoff and soil loss: a flume study." *Soil Sci. Soc. Am. J.*, 62(1), 243-250.

Hillel, D. (1998). *Environmental Soil Physics*. Academic Press, San Diego, CA.

Huang, C., and Bradford, J. M. (1990). "Portable laser scanner for measuring soil surface roughness." *Soil Sci. Soc. of Am. J.*, 54(5), 1402-1406.

Kacimov, A. R., Al-Ismaily, S., and Al-Maktoumi, A. (2010). "Green-Ampt one-dimensional infiltration from a ponded surface into a heterogeneous soil." *J. Irrig. Drain. E.*, ASCE, 136(1), 68-72.

Kamphorst, E. C., Chadœuf, J., Jetten, J., and Guérif, J. (2005). "Generating 3D soil surfaces from 2D height measurements to determine depression storage." *Catena*, 62(2-3), 189-205.

Kamphorst, E. C., and Duval, Y. (2001). "Validation of a numerical method to quantify depression storage by direct measurements on moulded surfaces." *Catena*, 43(1), 1-14.

Kamphorst, E. C., Jetten, V., Guérif, J., Pitkänen, J., Iversen, B. V., Douglas, J. T., and Paz, A. (2000). "Predicting depression storage from soil surface roughness." *Soil Sci. Soc. Am. J.*, 64(5), 1749-1758.

Loaiciga, H. A., and Huang, A. (2007). "Ponding analysis with Green-and-Ampt infiltration." *J. Hydrol. Eng.*, 12(1), 109-112.

Ma, Y., Feng, S., Su, D., Gao, G., and Huo, Z. (2010). "Modeling water infiltration in a large layered soil column with a modified Green-Ampt model and HYDRUS-1D." *Comput. Electron. Agr.*, 71(1), S04-S47.

Magunda, M. K., Larson, W. E., Linden, D. R., and Nater, E. A. (1997). "Changes in microrelief and their effects on infiltration and erosion during simulated rainfall." *Soil Technol.*, 10(1), 57-67.

Martin, Y., Valeo, C., and Tait, M. (2008). "Centimetre-scale digital representations of terrain and impacts on depression storage and runoff." *Catena*, 75(2), 223-233.

McClave, J., Sinich, T. (2009). *Statistic*. 11th ed. Pearson Prentice Hall, Upper Saddle River, NJ

Mein, R. G., and Larson, C. L., (1971). *Modeling infiltration component of rain-fall-runoff process*, Bulletin 43, Water Resources Research Center, University of Minnesota, Minneapolis, MN, 72 pp.

Mein, R. G., and Larson, C. L., (1973). "Modeling infiltration during a steady rain." *Water Resour. Res.*, 9(2), 384-394.

Mein, R. G., and Farrell, D. A. (1974). "Determination of wetting front suction in the green-ampt equation." *Soil Sci. Soc. Am. J.*, 38, 872-876.

Merz, B., and Plate, E. J. (1997). "An analysis of the effects of spatial variability of soil and soil moisture on runoff." *Water Resour. Res.*, 33(12), 2909-2922.

Meyer, L. D. (1994). "Rainfall simulators for soil erosion research." In: *Soil Erosion Research Methods*, 2nd Edition, edited by R. Lal. CRC Press.

Meyer, L.D., and Harmon, W. C. (1979). "Multiple-intensity rainfall simulator for erosion research on row sideslopes." *Transactions of the American Society of Agricultural Engineers*, 22, 100-103.

Mitchell, K. J., and Jones, B. A. (1976). "Micro-relief surface depression storage: analysis of models to describe the depth-storage function." *Water Resour. Bull.*, 12(6), 1205-1222.

Mualem, Y. (1976). "A new model for predicting the hydraulic conductivity of unsaturated porous media." *Water Resour. Res.*, 12(3), 513-522.

Neuman, S. P. (1976). "Wetting front pressure head in the infiltration model of Green and Ampt." *Water Resour. Res.*, 12(3), 564-566.

O'Callaghan, J. F., and Mark, D. M. (1984). "The extraction of drainage networks from digital elevation data." *Comput. Vision Graph.*, 28(3), 323-344.

Onstad, C. A. (1984). "Depressional storage on tilled soil surfaces." *Transactions of ASCE*, 27(33), 729-732.

Panikar, J. T., and Nanjappa, G. (1977). "Suction head at wet front in unsaturated-flow problems – a new definition." *J. Hydrol.*, 33, 1-14.

Philip, J. R. (1955). "Numerical solution of equations of the diffusion type with diffusivity concentration-dependent." *Trans. Faraday Soc.*, 51(7), 885-892.

Philip, J. R. (1957a). "Numerical solution of equations of the diffusion type with diffusivity concentration-dependent. II." *Australian Journal of Physics*, 10, 29-42.

Philip, J. R. (1957b). "The theory of infiltration: 1. The infiltration equation and its solution." *Soil Sci.*, 83, 345-357.

Rawls, W. J., and Brakensiek, D. L. (1982). "Estimating soil-water retention from soil properties." *J. Irrig. Drain. E.*, ASCE, 108(IR2), 166-171.

Rawls, W. J., and Brakensiek, D. L. (1983). "A procedure to predict Green and Ampt infiltration parameters." *Proc., Conference on Advances in Infiltration*, American Society of Agricultural Engineers, Chicago, IL, 102-112.

Rawls, W. J., Brakensiek, D. L., and Miller, N. (1983a). "Green-Ampt infiltration parameters from soils data." *J. Hydrol. Eng.*, 109(1), 62-70.

Rawls, W. J., Brakensiek, D. L., and Soni, B. (1983b). "Agricultural management effects on soil-water processes; Part I: Soil-water retention and Green and Ampt infiltration parameters." *Transaction of the American Society of Agricultural Engineers*, 26(6), 1747-1752.

Richards, L. A. (1931). "Capillary conduction of liquids through porous mediums". *Physics* 1(5): 318–333.

Rooij, G. H. (1999). "Modeling fingered flow of water in soils owing to wetting front instability: a review." *J. Hydrol.*, 231-232, 277-294.

Sande, L., Chu, X., and Desutter, T. (2011). "A new method for replicating complex microtopographic surfaces in laboratory soil box experiments." *Appl. Eng. Agric*, 27(4), 615-620.

Slack, D. C., and Larson, C. L. (1981). "Modeling infiltration: the key process in water management, runoff, and erosion." *Tropical Agricultural Hydrology*, John Wily & Sons Ltd., Chichester, Great Britain, 433-450.

Sullivan M., Warwick, J. J., and Tyler, S. W. (1996). "Quantifying and delineating spatial variation of surface infiltration in a small watershed." *J. Hydrol.*, 181(1-4), 149-168.

Tricker, A. S. (1981). "Spatial and temporal patterns of infiltration." *J. Hydrol.*, 49(3-4), 261-277.

Van Genuchten, M. Th. (1980). "A closed-form equation for predicting the hydraulic conductivity of unsaturated soils." *Soil Sci. Soc. Am. J.*, 44(5), 892-898.

Van Genuchten, M. Th., Leij, F. J., and Yates, S. R. (1991). *The RETC Code for Quantifying the Hydraulic Functions of Unsaturated Soils*. U.S. Salinity Laboratory, U.S. Department of Agriculture, Agricultural Research Service, Riverside, California, USA.

Van Mullen, J. A. (1989). *Application of the Green-Ampt infiltration model to watersheds in Montana and Wyoming*, M.S. thesis, Montana State University, Bozeman, MT.

Wei, L., Zhang, B., and Wang, M. (2007). "Effects of antecedent soil moisture on runoff and soil erosion in alley cropping systems." *Agr. Water Manage*, 94(1-3), 54-62.

Williams, J. R., Ouyang, Y., Chen, J., and Ravi, V. (1998). *Estimation of infiltration rate in the vadose zone: Application of selected mathematical models*, Vol. II, EPA/600/R-

97/128b, U.S. Environmental Protection Agency, National Risk Management Research Laboratory, Ada, OK, 1-117.

Wilson, B. N., Slack, D. C., and Larson, C. L. (1981). "An infiltration model: development and evaluation of its parameters." *Transactions of the American Society Agricultural and Biological Engineering*, 24 (3) 670-677.

Zhang, R. (1997). "Determination of soil sorptivity and hydraulic conductivity from the disk infiltrometer." *Soil Sci. Soc. Am. J.*, 61(4), 1024-1030.